Increasing Daily Extreme and Declining Annual Precipitation in Southern Europe: A Modeling Study on the Effects of Mediterranean Sea Warming

Alfonso Senatore[1], Luca Furnari[1], Gholamreza Nikravesh[1], Jessica Castagna[1], and Giuseppe Mendicino[1]
[1]Department of Environmental Engineering, University of Calabria, Rende 87036, Cosenza, Italy
Correspondence: Alfonso Senatore (alfonso.senatore@unical.it)

Abstract. Understanding the evolving patterns of intense rainfall in the Mediterranean under climate change is an urgent challenge. An analysis of the annual total and maximum one-day precipitation from 1955 to 2023 performed with the ERA5-Land dataset over the Mediterranean area reveals emerging patterns of contrasting trends along much of the northern Mediterranean coast, with heavy precipitation events increasing and total annual rainfall decreasing. An independent investigation on a ground-based dense monitoring network in southern Italy confirms the results. We focus on this representative sub-region of the study area to examine in detail the role of sea-atmosphere-orography interactions, particularly the impact of increasing sea surface temperature (SST), in enhancing heavy precipitation despite overall drying. Twenty consecutive precipitation events identified in a particularly intense rainy season (September-December 2019) are reproduced at a convection-permitting resolution (2 km) using the Weather Research and Forecasting (WRF) model with ERA5 reanalysis boundary conditions. Then, two scenarios are tested: one with past SST levels approximating 1980 and another with SST increases in line with end-of-century Shared Socioeconomic Pathways (SSPs) projections. WRF simulations thoroughly describe cyclone tracks and precipitation patterns, showing that increased SST boosts the frequency of heavy rainfall events overland. However, peak rainfall accumulations remain mostly unchanged because the highest precipitations occur over the sea. The study demonstrates the unique capability of high-resolution, convection-permitting analyses to capture complex processes in orographically challenging regions and contributes to clarifying the seemingly contradictory trend of rising daily precipitation extremes despite falling annual precipitation totals in Southern Europe.

1 Introduction

Observations from the last century confirm that the global warming trend has not had a uniform impact worldwide on local climates and hydrological cycles. The carbon dioxide-induced warming is more emphasized in the Arctic pole, especially in winter (Stone, 2021), but severe implications on weather can also be detected in the mid-latitudes of the Northern Hemisphere, where cold anomalies due to outbreaks of Arctic cold air are detected (Kömüşcü and Oğuz, 2021) and the expansion of the Hadley Cell is slightly faster than in the Southern Hemisphere (Xian et al., 2021). Generally, the atmospheric circulation of the thermally closed Hadley Cell pushes the warmer fluid from the equator polewards, while cold fluid is pushed towards the subtropics and equatorward. Over the last few decades, as confirmed by chemical metrics, the Hadley Cell has shown a poleward

trend, which may lead to more frequent droughts at higher latitudes (Xian et al., 2021). For instance, the Mediterranean area, as well as the Middle East, Western Pacific, and Asian monsoon regions, are hit by more frequent heatwave events due to the expansion of the Hadley Cell.

Among the subtropical regions, the Mediterranean Basin is a recognized climate change hotspot (Giorgi, 2006), subject of particular interest due to the high number of inhabitants living in this region and its importance in several historical, economic, and social aspects, but also because of the peculiarities of the observed and projected climate change signals (Tuel and Eltahir, 2020). In particular, Alpert et al. (2002) had already highlighted a paradox in the increase of extreme daily rainfall despite a decrease in total precipitation, which in statistical terms can be summarized as an "increase in variance" overcoming the "reduction in the mean" (Meehl et al., 2000). Such dichotomous behavior, concerning both observations and projections, has been confirmed and detailed in further studies (e.g., about mean reduction: Lionello and Scarascia 2018; Tuel and Eltahir 2020; Zappa et al. 2015; Babaousmail et al. 2022; about variance increase: Zappa et al. 2015; Zittis et al. 2021; Avino et al. 2024; while Lazoglou et al. 2024 adopted an approach identifying the spatial distribution of both trends).

The geographical and climatological peculiarities of the Mediterranean Basin contribute to a further increase in Sea Surface Temperature (SST), accelerating the effects of global warming (Pastor et al., 2020). The annual warming rate recorded in Mediterranean SST is about 0.35 °C/decade, corresponding to a rate increase of about 1.3 °C from 1982 to 2019 (Pastor et al., 2020; Mohamed et al., 2019) for the whole basin, with a maximum rate in the Eastern basin (0.40 °C/decade), and lower rates related to the western and central basin (0.35 °C/decade and 0.31 °C/decade, respectively) (Pastor et al., 2020; Sannino et al., 2022). In 2023 and 2024, the recorded Mediterranean Sea SST was the highest since the 1950s (Cheng et al., 2024, 2025).

Moreover, the Mediterranean region is generally affected by significant cyclonic activity, which can even lead to the formation of tropical-like cyclones, known as Medicanes (Miglietta and Rotunno, 2019; Flaounas et al., 2022; Miglietta et al., 2025), characterized by destructive winds and torrential rainfall. For instance, frequent extreme precipitation events caused by Medicanes were recorded in Europe between 1979 and 2017, among which over 20 occurred in Italy, followed by France, Croatia, Serbia, and Greece (Zhang et al., 2021). However, in the very recent years, the whole region has experienced several extreme events with severe consequences, whether they were classified as Medicanes (e.g., the Storm Daniel in Libya in 2023, Armon et al. 2025; Flaounas et al. 2024), cut-off low pressure systems (the Valencia event in Spain in 2024, Amiri et al. 2025) or persistent depression vortexes (the two consecutive events in Emilia Romagna (Italy) in 2023 and 2024, Arrighi and Domeneghetti 2024; Ferrari et al. 2025), all of which were correlated to particularly high SST values.

From the point of view of physics, cyclogenesis processes are influenced by thermodynamical and dynamical factors. Thermodynamically, the SST warming, which defines the air-sea heat flux, leads to larger evaporation and more moisture content, especially in the lower Planetary Boundary Layer (PBL) and in a minor part in the upper PBL (Khodayar et al., 2021; Sun and Wu, 2022). Additionally, the effects of increased moisture may dynamically interact with orographic lifting, causing deep convection, an increase in Convective Available Potential Energy (CAPE), and, as a final result, extreme precipitation events (Müller et al., 2024; Ricchi et al., 2023; Pfahl et al., 2017; Meredith et al., 2015).

The increasing trend of the Mediterranean SST is predicted to continue. Future scenario projections of SST suggest additional warming. As an example, under RCP8.5, an increase of over 3 °C is predicted (+3.31 °C for 2081-2100 related to the

upper layer 0-100 m for the whole Mediterranean Basin, +2.98 °C for the western basin, and +3.50 °C for the eastern basin) (Sannino et al., 2022). On the other hand, the spatial patterns of future precipitation trends are more heterogeneous and complex to detect. The great challenge of deciphering how global warming will affect rainfall at local scales (Chadwick, 2017) is particularly tough in regions with transitional climate regimes, such as the Mediterranean. In the subtropics, a large-scale precipitation decline is generally projected (He and Soden, 2017). However, the indications about how this phenomenon will affect local areas can be different depending on whether one relies on analyses at low spatial resolutions, such as GCMs (General Circulation Models) (Pfahl et al., 2017), or gradually increasing through climatic downscaling (Tramblay and Somot, 2018; Hosseinzadehtalaei et al., 2020; Reale et al., 2022; Matte et al., 2022) up to convection-permitting resolutions (Müller et al., 2024).

Several studies have evaluated the SST's strong influence on cyclonic activity in the Mediterranean, as well as on Medicanes. As intuitively expected, with a negative SST anomaly, cyclones are weaker, while in warmer SST conditions, precipitation increases (Miglietta et al., 2011; Meredith et al., 2015; Ricchi et al., 2017, 2023; Varlas et al., 2023). However, even slight uniform variations in SST ($\pm$0.5 °C) can influence precipitation patterns under particular synoptic conditions (Senatore et al., 2014). Similarly, it has been shown that a larger variation of SST from -2 °C to +2 °C strongly affects extreme events, such as in the case of cyclone Ianos (Varlas et al., 2023) that occurred in 2020, which produced a variation of precipitation intensity from -56% to +44% and influenced the tracks and the landfall location. Additionally, the high-resolution representation of the SST pattern reveals a weak but not negligible impact on operational forecasting results in many cases (Ricchi et al., 2017; Senatore et al., 2020b; Pilatin et al., 2021), contributing to the overall uncertainty along the modeling chain (Senatore et al., 2020a).

So far, the majority of the studies that aimed at disentangling the SST effect on precipitation in the Mediterranean basin using high-resolution simulations have restricted their analysis to a limited number of events (e.g., Meredith et al. 2015; Stocchi and Davolio 2017; Ricchi et al. 2023), focusing in particular on tropical-like cyclones (Fita et al., 2007; Miglietta et al., 2011; Ricchi et al., 2017; Noyelle et al., 2019; Varlas et al., 2023). To the authors' knowledge, only Armon et al. (2022) performed a systematic analysis by identifying 41 extreme events hitting the eastern Mediterranean over 24 years starting from 1990, and comparing them with "pseudo-global warming" (e.g., Rasmussen et al. 2011) simulations, in which the climate change signal related to the end-of-21st-century RCP8.5 scenario was added to several historical variables besides SST, including the whole skin temperature, surface pressure, and 3D fields of temperature, wind, and specific humidity.

The climate of Southern Europe, whose coastline broadly faces the central/western Mediterranean Sea, is influenced on the one hand by the SST and on the other hand by an often locally complex orography with steep mountains opposing atmospheric water transport, both conditions rendering this region prone to extreme precipitation events characterized by strong air-sea-orography interactions (Berthou et al., 2016; Senatore et al., 2020b). A systematic analysis of the effects of Mediterranean Sea warming on the intensity and location of weather events of different sizes affecting this region, with particular reference to their impact overland, is lacking, although it is necessary for adequate preparation for water resource management and land protection under ongoing climate change.

In this study, we first analyzed current trends of intense precipitation considering maximum one-day observations for the whole Euro-Mediterranean region, and compared them with total annual precipitation trends to disentangle possible contrasting behaviors of the two variables, therefore verifying and updating the information about the decreasing mean/increasing variance paradox highlighted by Alpert et al. (2002). To this aim, we used the data provided by the ERA5-Land dataset (Muñoz-Sabater et al., 2021) over the EURO-CORDEX domain (Jacob et al., 2014). The robustness of the results achieved with the large-scale reanalysis in the Mediterranean area was then tested with local observations from a dense ground-based monitoring network available in the southernmost part of the Italian peninsula, corresponding to the administrative region of Calabria, located almost at the geographical center of the Mediterranean Sea. Calabria's unique geography, with steep orography and surrounding seas, creates conditions highly favorable to extreme precipitation. Interactions between intense air–sea exchanges and coastal topography amplify local instabilities. As climate change advances, this area faces frequent and severe extreme precipitation events, making it a challenging and significant testbed in the Mediterranean Basin (Mastrantonas et al., 2022). The comparison between the reanalysis and local observations showed general agreement between the two datasets, further confirming the regional representativeness of the Calabrian Peninsula. Afterwards, to explain the current and future influence of SST on the dynamics and intensity of precipitation events in Southern Europe, we focused on this representative sub-region, considering for the first time a set of 20 real-world events with different intensity that occurred during a particularly heavy rainy season (from September to December 2019) and reproducing them at convection-permitting scale (2 km) using the WRF (Weather Research and Forecasting, Skamarock et al. 2021) model with boundary conditions provided by ERA5 reanalysis for two nested domains. Successively, while preserving the other boundary conditions, we performed a sensitivity analysis with calibrated SST lower boundary conditions for two scenarios: a past scenario with a decrease in SST equivalent to the SST recorded approximately in 1980, and a scenario with an increase reasonably representative of the projections for the end of this century according to selected Shared Socioeconomic Pathways (SSPs) scenarios. The overall analysis, which specifically focused on the impact on land areas, provided a comprehensive insight into the evolution of heavy precipitation intensity and frequency in the northern coastal Mediterranean and its correlation to sea surface warming.

2 Data and Methods

2.1 Datasets and study area

For the historical trend analysis at the Euro-Mediterranean level, the ERA5-Land data were used for the 69 years from 1955 to 2023. The ERA5-Land dataset is an enhanced global land dataset at 0.1° resolution derived from the 5^{th} generation of European ReAnalysis (ERA5), produced by the European Centre for Medium-Range Weather Forecasts (ECMWF) in the framework of the Copernicus Climate Change Service (C3S) (Muñoz-Sabater et al., 2021). ERA5-Land data were chosen because of their relatively high resolution and the concurrent availability of coherent precipitation and temperature data. Furthermore, ERA5-Land proved to be generally reliable in the selected domain (Muñoz-Sabater et al., 2021; Cammalleri et al., 2022; Vanella et al., 2022; Gomis-Cebolla et al., 2023; Ippolito et al., 2024).

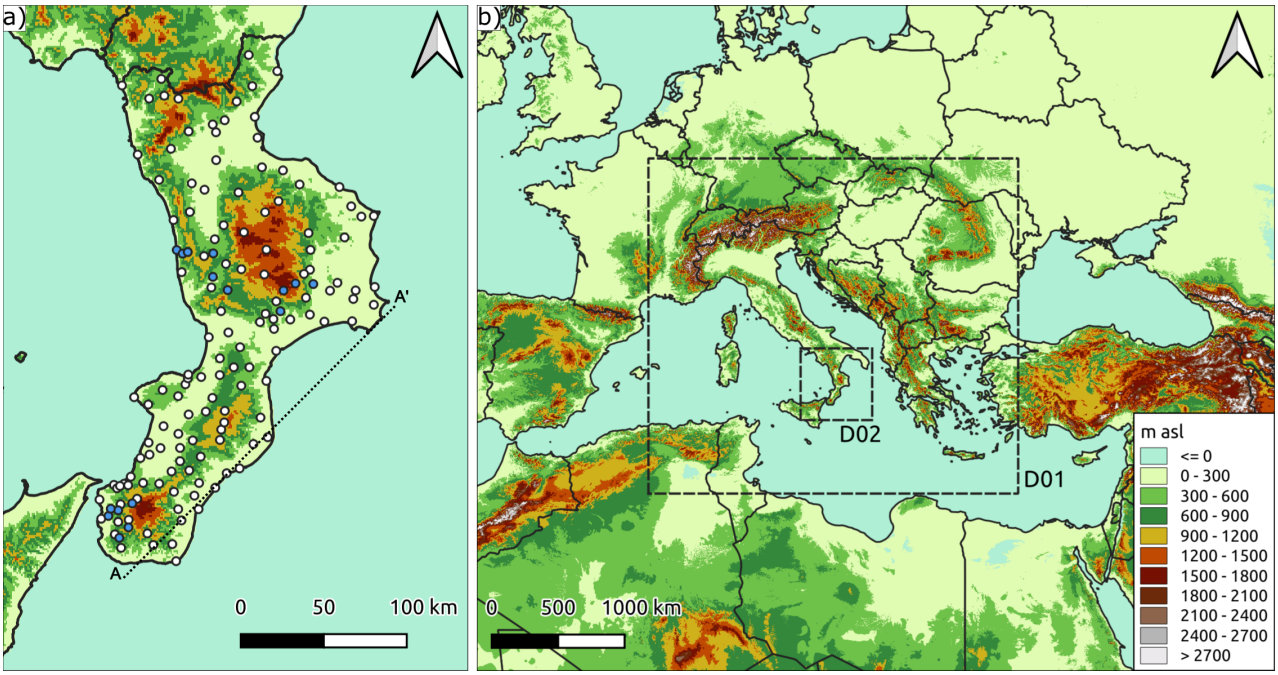

Figure 1. a) Overview of the Calabria Region with the administrative borders (bold black lines) and the location of the 134 historical precipitation gauges used for the trend analysis (white dots). In addition, 16 other gauges were used for the 2019 spatial precipitation distribution (blue dots). The vertical water vapor fluxes are calculated across section A-A' (Fig. 15); b) Topographic map of the Central Mediterranean area showing the two outermost (D01) and innermost (D02) WRF domains.

The results based on the ERA5-Land dataset were compared at the local scale, considering the southernmost peninsula of Italy, which corresponds to the administrative region of Calabria. Calabria Region (Fig. 1a) covers an area of 15080 km^2 that lies between $37°54'$ and $40°09'$N and $15°37'$ and $17°13'$E. The profound influence of the surrounding sea on atmospheric conditions, combined with the complex local orography, makes the Calabrian climate highly heterogeneous, with sharp transitions from humid to dry areas (Mendicino and Versace, 2007; Senatore et al., 2020a). The peculiar physical characteristics of the territory not only make it prone to drought risk (generally higher in the eastern part) but contribute to the development of extreme and damaging hydrometeorological events on both eastern (Ionian) and western (Tyrrhenian) coasts, especially during the late summer until the late fall season when considerable amounts of precipitation in a short time cause severe floods with economic and social damages, including fatalities (e.g., Llasat et al. 2013; Petrucci et al. 2018; November 2015 - Avolio and Federico 2018; November 2016 - Senatore et al. 2020a; November 2019 - Furnari et al. 2022). Daily precipitation data were collected in Calabria from 134 gauges (roughly a gauge per 110 km^2) of the regional monitoring network (Fig. 1a). To estimate missing values or reconstruct detected outliers, a linear correlation process was applied as follows: (i) daily rainfall data were collected for each station from 1955 to 2023. If fewer than 15 days were missing in a given year (approximately 4%, as suggested in several studies, e.g., Aguilar et al. 2005; Donat et al. 2013; Stephenson et al. 2014), the dataset for that year

was considered complete. (ii) If more than 15 days were missing for a station in a given year, we performed a linear regression between that station's available data and the data from a nearby station with a strong correlation (always above 0.8, often much higher). The regression equation was then used to fill the gaps. While this approach could influence extreme-event values, we applied it cautiously, taking into account the characteristics of the data.

The season most prone to extreme hydrometeorological events in southern Italy is the fall (from September to December) when cold-air intrusions reach the marine boundary layer with still high SST (Noyelle et al., 2019). For example, during the 2019 fall season, 20 precipitation events were recorded in southern Italy, among which two extreme events (from 11th to 13th of November, Marsico and Rotundo 2019, and from 23rd to 25th of November, Fusto et al. 2019) produced very intense precipitations (more than 200 mm of accumulated precipitation in some locations) and powerful wind speeds (gusts of up to 100 km/h), causing severe floods. Therefore, the period from September to December 2019 was selected as a case study to assess the sensitivity of the events to varying SST boundary conditions. For this period, it was possible to benefit from new gauges, increasing the size of the ground-based observations to 150 gauges (Fig. 1a). Precipitation data were spatially interpolated using inverse distance weighting (IDW) at the same resolution as the atmospheric model, allowing for easier comparison with its spatially distributed output. Although including ungauged (interpolated) areas in the evaluation introduces some uncertainty, three points are worth noting: (i) a single gauge may not fully represent the model grid cell where it lies, especially in steep terrain so that also gauge-to-pixel comparisons can be biased; (ii) the region's dense monitoring network limits major misinterpretations of spatial precipitation patterns; and (iii) the fully validated observational dataset is the most reliable basis for constructing a gridded dataset.

We used several datasets to analyze the observed and projected SST values of the Mediterranean Sea, assessing a reasonable range of variations in the atmospheric model's boundary conditions. As observed data, the 5th generation ECMWF reanalysis, i.e., the monthly SST ERA5 reanalysis from 1980 to 2023, combining global model data with observations sampled globally, was selected. We also used the Copernicus Marine Service (CMEMS) observations (SST-GLO-SST-L4-REP-OBSERVATIONS-010-011, ID: ESACCI-GLO-SST-L4-REP-OBS-SST, C3S-GLO-SST-L4-REP-OBS-SST) on a daily scale from 1982 to October 2022, based on the reprocessing analysis of satellite and in-situ data. The spatial extensions of the analyzed region correspond to the external domain of the weather simulations (Section 2.3).

Regarding SST projections, we utilized the internationally coordinated Coupled Model Intercomparison Project Phase 6 (CMIP6), which provides 22 GCM (Global Circulation Model) results (Table 1). The projections selected belong to two different Shared Socioeconomic Pathways (SSPs, Meinshausen et al. 2020) scenarios:

- the medium-high emission scenario, i.e., SSP3-7.0 (called Regional Rivalry) characterized by high GHG emissions and CO_2 doubling around current levels until the end of the century;
- the worst scenario, SSP5-8.5 (named Fossil-Fueled Development - Taking the Highway) with very high GHG emissions and CO_2 that roughly triple from current levels by 2075.

Table 1. List of datasets (IDs 0_1 and 0_2) and GCMs (IDs 1-22) considered for assessing observed/estimated historical and estimated future SST evolution in the Mediterranean Area. GCMs data have been provided by Instituto de Física de Cantabria (IFCA)

ID	Complete Name	Institution	Model	Variant	Reference
0_1	ERA5 Reanalysis	ECMWF	Reanalysis		Hersbach et al. (2020)
0_2	SST_GLO_SST_L4_REP_OBSERVATIONS_010_024	CMEMS	Observation		(CMEMS) (2023)
1	ACCESS-CM2_CSIRO-ARCCSS_r1i1p1f1	CSIRO-ARCCSS	ACCESS-CM2	r1i1p1f1	Dix et al. (2023)
2	ACCESS-ESM1-5_CSIRO_r1i1p1f1	CSIRO	ACCESS-ESM1-5	r1i1p1f1	Ziehn et al. (2023)
3	AWI-CM-1-1-MR_AWI_r1i1p1f1	AWI	AWI-CM-1-1-MR	r1i1p1f1	Semmler et al. (2023)
4	BCC-CSM2-MR_BCC_r1i1p1f1	BCC	BCC-CSM2-MR	r1i1p1f1	Xin et al. (2023)
5	CAMS-CSM1-0_CAMS_r2i1p1f1	CAMS	CAMS-CSM1-0	r2i1p1f1	Rong (2023)
6	CESM2-WACCM_NCAR_r1i1p1f1	NCAR	CESM2-WACCM	r1i1p1f1	Danabasoglu (2023)
7	CMCC-CM2-SR5_CMCC_r1i1p1f1	CMCC	CMCC-CM2-SR5	r1i1p1f1	Lovato and Peano (2023)
8	CNRM-CM6-1-HR_CNRM-CERFACS_r1i1p1f2	CNRM-CERFACS	CNRM-CM6-1-HR	r1i1p1f2	Voldoire (2023a)
9	CNRM-CM6-1_CNRM-CERFACS_r1i1p1f2	CNRM-CERFACS	CNRM-CM6-1	r1i1p1f2	Voldoire (2023b)
10	CNRM-ESM2-1_CNRM-CERFACS_r1i1p1f2	CNRM-CERFACS	CNRM-ESM2-1	r1i1p1f2	Seferian (2023)
11	CanESM5_CCCma_r1i1p1f1	CCCma	CanESM5	r1i1p1f1	Swart et al. (2023)
12	EC-Earth3_EC-Earth-Consortium_r1i1p1f1	EC-Earth-Consortium	EC-Earth3	r1i1p1f1	(EC-Earth)
13	FGOALS-g3_CAS_r1i1p1f1	CAS	FGOALS-g3	r1i1p1f1	Li (2023)
14	GFDL-ESM4_NOAA-GFDL_r1i1p1f1	NOAA-GFDL	GFDL-ESM4	r1i1p1f1	Krasting et al. (2023)
15	IITM-ESM_CCCR-IITM_r1i1p1f1	CCCR-IITM	IITM-ESM	r1i1p1f1	Panickal et al. (2023)
16	INM-CM5-0_INM_r1i1p1f1	INM	INM-CM5-0	r1i1p1f1	Volodin et al. (2023)
17	IPSL-CM6A-LR_IPSL_r1i1p1f1	IPSL	IPSL-CM6A-LR	r1i1p1f1	Boucher et al. (2023)
18	MPI-ESM1-2-HR_MPI-M_r1i1p1f1	MPI-M	MPI-ESM1-2-HR	r1i1p1f1	Jungclaus et al. (2023)
19	MPI-ESM1-2-LR_MPI-M_r1i1p1f1	MPI-M	MPI-ESM1-2-LR	r1i1p1f1	Wieners et al. (2023)
20	NorESM2-LM_NCC_r1i1p1f1	NCC	NorESM2-LM	r1i1p1f1	Seland et al. (2023)
21	NorESM2-MM_NCC_r1i1p1f1	NCC	NorESM2-MM	r1i1p1f1	Bentsen et al. (2023)
22	UKESM1-0-LL_MOHC_r1i1p1f2	MOHC	UKESM1-0-LL	r1i1p1f2	Tang et al. (2023)

Although the likelihood of these intermediate to very high warming scenarios is debated (e.g., Schwalm et al. 2020; Hausfather and Peters 2020), they were taken into account to highlight as much as possible the effects of climate change on SST and indirectly on precipitation events driven by sea surface-atmosphere interaction.

2.2 Trend analysis

The non-parametric trend tests of Mann-Kendall (identifying significance at a 5% level) and Sen's slope estimator (determining the trend slope per year) were employed to analyze long-time hydro-climatic series of annual precipitation (PRCPTOT) and maximum one-day precipitation (RX1day). Mann (1945) formulated a non-parametric trend detection test, whereas the test statistic distribution was given by Kendall (1948) for turning point and non-linear trend assessment. This test aims to determine how independently and randomly the data are ordered by comparing the rank order of observations with their time order, considering the null hypothesis of no trend and serial structure in correlations (Hamed and Rao, 1998). Concerning the slope

estimator test, instead of the least squares estimator of a regression coefficient, the unbiased point estimator was defined based on the median of the set of slope joining pairs of points by Sen (1968).

To further clarify the joint behavior of the two variables, a rectangular two-axis coordinate system can be adopted. This representation enables a more systematic classification of compound trends. Within this framework, four distinct zones are defined based on whether the two variables exhibit concordant positive/negative trends or discordant trends. As Fig.2 shows, when PRCPTOT and RX1day trend values are assigned to the X- and Y-axes, respectively, Zone I (first quadrant) corresponds to the case in which both indices exhibit positive trends, Zone III (third quadrant) corresponds to the case in which both exhibit negative trends, and so on.

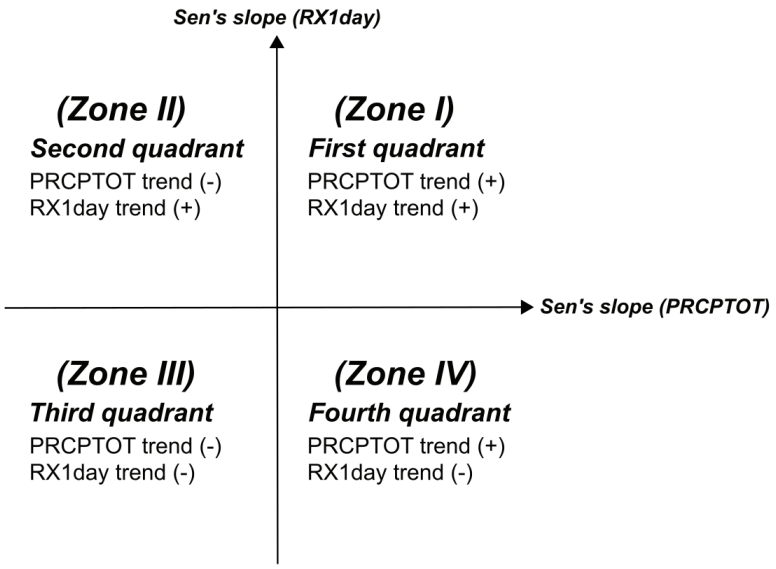

Figure 2. Quadrant classification diagram based on Sen's slopes of PRCPTOT and RX1day.

2.3 WRF downscaling and validation

Weather simulations over the Calabrian region were performed using WRF V4.1. Two one-way nested domains were used (see Fig. 1b): the outermost (D01) centered on the Italian peninsula, with a horizontal resolution of about 10 km ($33.04 - 49.85°$N, $3.59 - 28.59°$ E, thus producing 187×205 grid points); the innermost (D02) centered on the Calabrian region, with 2 km as horizontal resolution ($37.10 - 40.87°$ N, $13.88 - 18.71°$ E, 200×200 grid points). Both domains were extended on 44 vertical atmospheric layers, up to 50 hPa, and four soil layers. The time step size was set to 60 s and 12 s for the D01 and D02 domains, respectively. The physical scheme configuration (Table 2) is the same as that adopted by Avolio et al. (2019), with the replacement of NOAH-MP for NOAH as the Land Surface Model. This configuration has been operational for weather forecasting as an online service managed by the University of Calabria since 2020 (https://cesmma.unical.it/cwfv2/).

Table 2. WRF physical schemes adopted.

Component	Scheme	References
Microphysics	New Thompson	Thompson et al. (2008)
PBL	MYJ	Janjić (1994)
Longwave	RTTM	Mlawer et al. (1997)
Shortwave	Goddard	Matsui et al. (2020)
Land Surface Model	NOAH-MP	Niu et al. (2011)
Cumulus	Tiedke (only D01)	Tiedtke (1989)
SST	sst_skin	Zeng and Beljaars (2005)

The initial and boundary conditions were provided by ERA5 using the pressure levels mode; specifically, the following levels were used: 1000, 950, 900, 850, 800, 700, 600, 500, 400, 300, 200, 150, 100, and 50 hPa. The update frequency of the boundary conditions was set to three hours. The simulations started on the 1st of September 2019 and went on until the 1st of January 2020.

To perform the sensitivity analysis with respect to sea surface temperature, in addition to the reference simulation, we carried out two further experiments. In these experiments, the SST boundary conditions from ERA5 were uniformly modified (increased or decreased) in both domains, D01 and D02, based on evidence from historical observations (lower SST values) and GCM projections (higher SST values). The magnitude of the cold and warm SST perturbations, the method used to calculate them, and the rationale for their selection are described in the Results section 3.2. Furthermore, regarding warm SST perturbations, we ensured that the addition of a relevant quantity of energy to the modelled system did not significantly alter the larger-scale dynamics, patterns, and feedback. Therefore, we created another set of simulations in which we applied spectral nudging to the outer domain (D01) on the geopotential (ERA5 source) at heights above 500 m, as done in Meredith et al. (2015). New experiments, shown in the Supplementary (Fig. S1), ensured consistency of the large-scale structures with respect to ERA5 and confirmed the robustness of the analysis.

The model performances were evaluated using two classical weather forecast indices: the Fractional Skill Score (FSS) and the Critical Success Index (CSI), also referred to as the Threat Score (TS) (Wilks, 2006). The FSS (Eq. 1) ranges from 0 (mismatch) to 1 (perfect match) and highlights how the spatial pattern forecasted could match with respect to the observed one. Assuming a square-shaped neighborhood of length (size) n, FSS_n is given by:

$$FSS_n = 1 - \frac{\frac{1}{N}\sum_{i=1}^{N}\left(P_f - P_o\right)^2}{\frac{1}{N}\left[\sum_{i=1}^{N}P_f^2 + \sum_{i=1}^{N}P_o^2\right]} \tag{1}$$

In the above equation, N is the number of windows in the domain, and P_f and P_o are boolean values indicating if the pixel value is higher or lower than the threshold related to the observation. We applied the FSS by considering the events identified according to the procedure described in the next section 2.4 and using the 90th percentile on the cumulative precipitation

observed as the threshold. Moreover, according to Senatore et al. (2020a), we calculated the FSS only for the Calabrian peninsula, where we collected and interpolated highly reliable spatial data, excluding the sea.

The CSI (Eq. 2) quantifies the fraction of observed and forecasted events that are correctly predicted by varying the rainfall thresholds. The index varies between 0 (no skill) and 1 (perfect skill):

$$CSI = \frac{hits}{hits + misses + false\ alarms} \tag{2}$$

We considered the observed and predicted precipitation cell by cell during the events to build up the contingency table by varying the thresholds, whose selected values were 0.2, 0.5, 1, 2, 5, 10, 20, and 30 mm.

2.4 Space and time events identification and evaluation of the effects of the SST scenarios

During the selected period from September to December 2019 for WRF simulations, the spatial average of the simulated daily precipitation over the inner domain with actual SST boundary conditions was used to identify and label the events that occurred. Each event was objectively recognized by using a fixed threshold of 0.8 mm on the average daily precipitation values simulated by the WRF reference run over the Calabria region. This procedure ensured that each event was treated as independent from the others. The analysis was based on the reference simulation rather than on actual observations, as the simulation proved highly reliable in terms of event timing and facilitated subsequent comparisons with the SST sensitivity experiments.

The precipitation patterns for the current SST and modified SST scenarios were also evaluated. In particular, since we were interested in the localization of the precipitation peaks, for each event and given SST boundary condition, we calculated the positions of the barycenters of the areas where the accumulated precipitation exceeded the 95th percentile. Specifically, the barycenters were calculated by considering all grid points in which the accumulated precipitation during the event was greater than the 95th percentile, according to the equations reported below:

$$x = \frac{\sum_{i=1}^{N} Prec(i,j) * i}{\sum_{i=1}^{N} Prec(i,j)} \tag{3}$$

$$y = \frac{\sum_{j=1}^{N} Prec(i,j) * j}{\sum_{j=1}^{N} Prec(i,j)} \tag{4}$$

In the above equations, i and j indicate the indices of each of the N pixels exceeding the 95th percentile threshold, while $Prec(i,j)$ is the accumulated precipitation value in the pixel with coordinates (i,j). Finally, x and y are the coordinates of the barycenter of the precipitation event.

Finally, to quantitatively assess the effect of the different SST scenarios, we calculated the SAL metrics (Wernli et al., 2008) for each of the 20 events, considering the entire inner domain and the SST0 scenario as a reference. The SAL method comprises three components: the Structure component assesses whether the spatial patterns in the considered field align with

the reference ones, focusing on the shape of the precipitation areas, specifically whether they are too smooth (negative values) or too peaked/fragmented (positive values). Amplitude compares the average intensity, checking for over- (positive values) or under-estimation (negative values). Location evaluates the distance by which the precipitation fields are displaced, focusing on the centers of mass.

3 Results

3.1 Trend Analysis

Even though the Sen's slope and Mann-Kendall trend test for PRCPTOT and RX1day were calculated over the whole EURO-CORDEX domain, for the sake of clarity, the results are shown only for the Mediterranean area (30° to 50° N and 15° W to 45° E, Fig. 3). In general, eastern and southern regions of Europe are experiencing decreasing trends of PRCPTOT (Fig. 3a), unlike the central and northern territories of the continent (only partially shown in the Fig.). Negative trends also affect most of North Africa. On the other hand, the RX1day trend is more scattered but overall slightly increasing, with approximately an average of 0.1 mm/year (Fig. 3b). The areas with significant trends are a minority (17.2% and 10.1% of the whole area, for PRCPTOT and RX1day, respectively), and are also widespread in space.

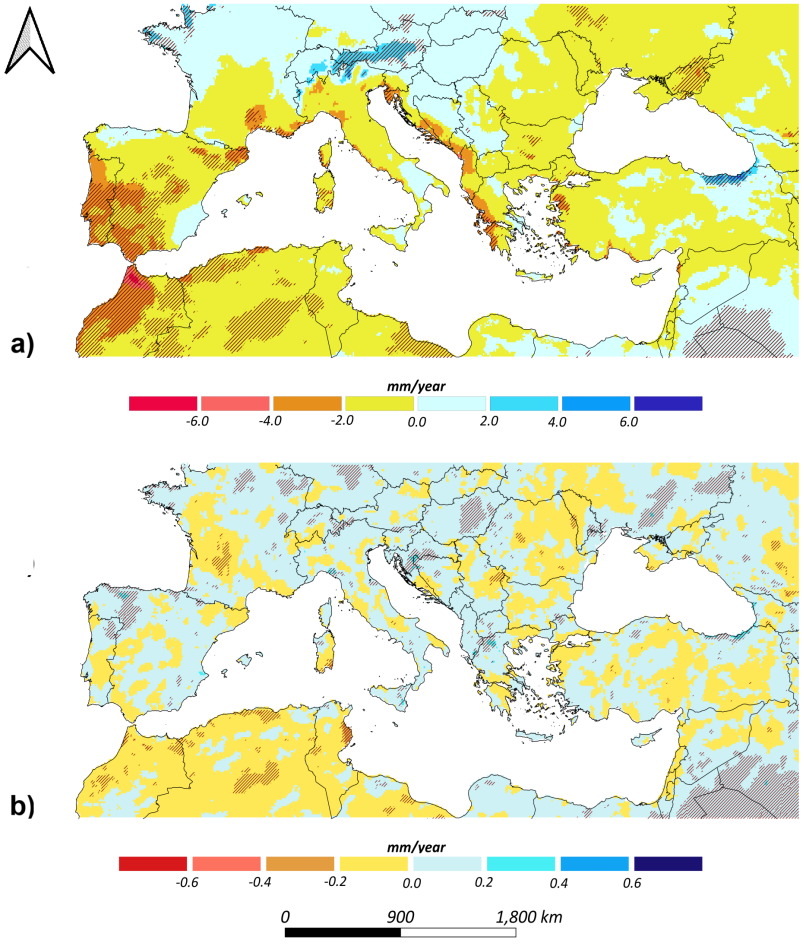

Figure 3. Mann-Kendall and Sen's slope (mm/year) tests for PRCPTOT (a) and RX1day (b) over the Mediterranean area, using ERA5-Land data from 1955 to 2023. Dashed areas highlight significant trends.

The assessment of combined trends is particularly interesting. Figure 4 presents the spatial distribution of the areas falling in the four quadrants of a two-dimensional domain where the horizontal axis represents the PRCPTOT trend, and the vertical axis represents the RX1day trend. 18,116 pixels out of about 69,000 land pixels (26%) are classified in the first quadrant (Zone I), where both PRCPTOT and RX1day trends are positive. Similarly, 22,735 (33%) and 24,727 (36%) pixels are placed in the second and third quadrants (Zones II and III), respectively, while the number of pixels belonging to the fourth quadrant (Zone IV) is the least (5%). Generally, the northern part of the study area (roughly, central Europe) is characterized by an increasing trend of both extreme and mean precipitation (Zone I). The same trend occurs for the areas in the southeastern corner of the domain (of course, in these dry areas, lower amounts of total precipitation are involved). In contrast, the southern regions of Europe and, to some extent, the eastern areas are experiencing a decreasing PRCPTOT trend (hence, higher drought risk) and

an increasing RX1day trend (which could contribute to higher flood risk) (Zone II). Other Eastern European areas, as well as most of the southern Mediterranean coasts, are experiencing a generalized decrease in trends (Zone III).

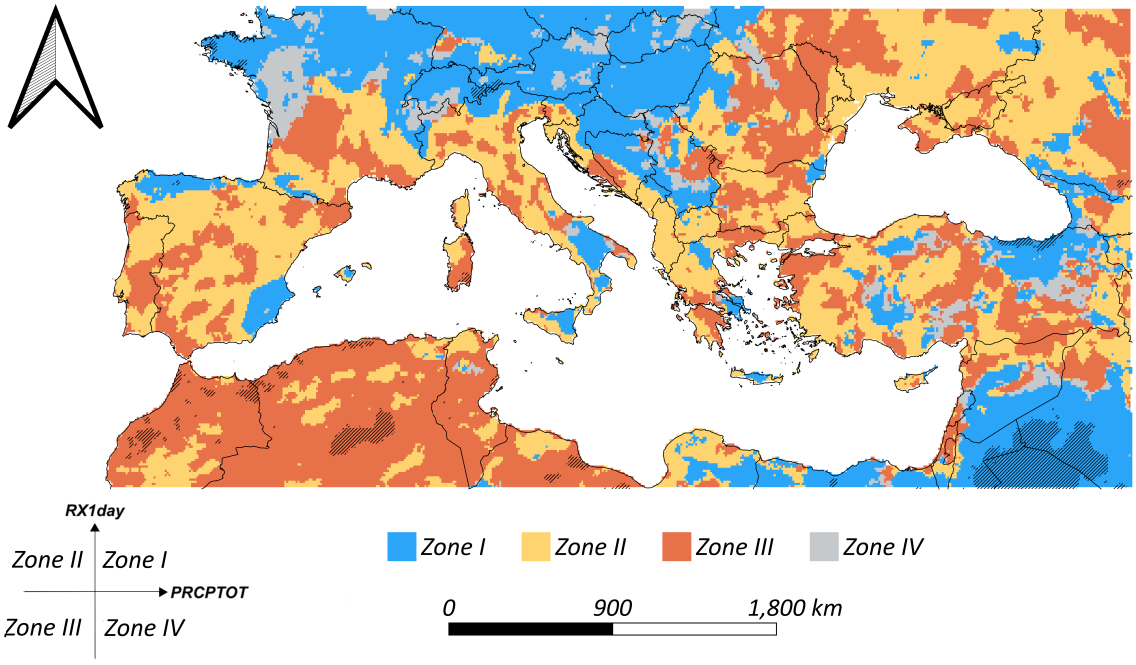

Figure 4. Four zones of compound trends of PRCPTOT and RX1day at annual scale over the Mediterranean region, using ERA5-Land data from 1955 to 2023, according to the diagram shown in Fig. 2. Dashed areas indicate that both PRCPTOT and RX1day trends are significant. The quadrant classification diagram is reproduced for the reader's convenience in the bottom-left corner of the Fig..

The results obtained with the ERA5-Land reanalysis dataset were compared locally with ground-based observations in the Calabrian Peninsula. Of the 134 stations considered, 29 were recognized with PRCPTOT significant negative trends (Fig. 5a), while four stations showed a significantly positive trend. In contrast, only eight stations (6% of the total) with significantly positive trends were found concerning RX1day (Fig. 5b), and even fewer stations (3, 2% of the total) with significant negative trends. Though the general behavior across the region is relatively straightforward, with the majority of the stations exhibiting negative PRCPTOT trends and positive RX1day trends, we performed a further analysis on how geographical and orographic factors —latitude, longitude, elevation, slope, aspect, and distance from the sea— affect average annual precipitation as well as PRCPTOT and RX1day trends. Using the k-means method within a Principal Component Analysis (PCA) framework, we divided the study area into four homogeneous clusters (Fig. S2, supplementary material). The results (Table S1) show that orography has a significant influence on the spatial distribution of precipitation, according to several previous studies (e.g., Colacino et al. 1997; Federico et al. 2009; Buttafuoco et al. 2011; Avolio and Federico 2018). Instead, no significant correlations emerged for the temporal trends of PRCPTOT and RX1day.

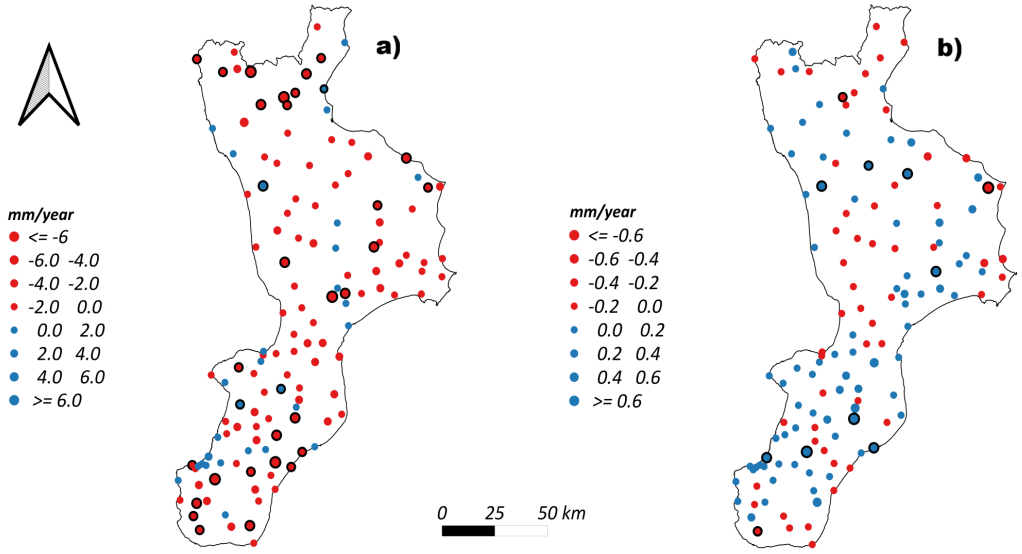

Figure 5. Mann-Kendall and Sen's slope tests for observations of a) PRCPTOT, b) RX1day over Calabria from 1955 to 2023. Black-contoured dots represent stations where trends are statistically significant.

The four zones of combined PRCPTOT and RX1day trends are depicted in Fig. 6. Nearly half of the stations (55, corresponding to 41.0%) are located in Zone (quadrant) II, facing an increasing risk of drought and extreme precipitation. Then, Zone III (both decreasing PRCPTOT and RX1day) is noticed with 50 stations (37.3%), whereas 23 stations (17.2%) are identified in Zone I. Finally, only six stations (4.5%) are placed in Zone IV. Only the stations with both significant PRCPTOT and RX1day trends are highlighted as "significant" in the maps. They are very few, with one station in Zones I and II and three in Zone III. Overall, the results indicate that Calabria primarily confronts a higher water stress risk, with a reduction in PRCPTOT detected in 105 stations, mostly accompanied by a temperature increase (not shown). Nevertheless, the risk of extreme precipitation events is not decreasing in the majority of the region (78 stations), with broad clusters of increased compound risk in the south, east, and northwest of the area (Zone II in Fig. 6).

Despite the differences (a gridded re-analysis at a 0.1° resolution vs. local-scale ground observations), the indications provided by the two datasets are generally convergent. According to Fig. S3, which shows the Sen's slope overlays extracted from both data sets for PRCPTOT (left panel) and RX1day (right panel), the percentages of ERA5-Land pixels and station-based positive trends in Calabria are quite similar for PRCPTOT (30.2% and 21.6%, respectively). In contrast, regarding RX1day, the ERA5-Land increasing trend percentage (92.2%) overestimates that provided by the gauge network (58.2%). Examining the spatial distribution of the trends, the ERA5-Land dataset reveals two main differences compared to observations: regarding PRCPTOT, it exhibits a bias towards positive trends in some mountainous areas; regarding RX1day, it provides an almost uniform positive trend. However, the level of agreement between the ERA5-Land pixels and the overlying stations (i.e., both

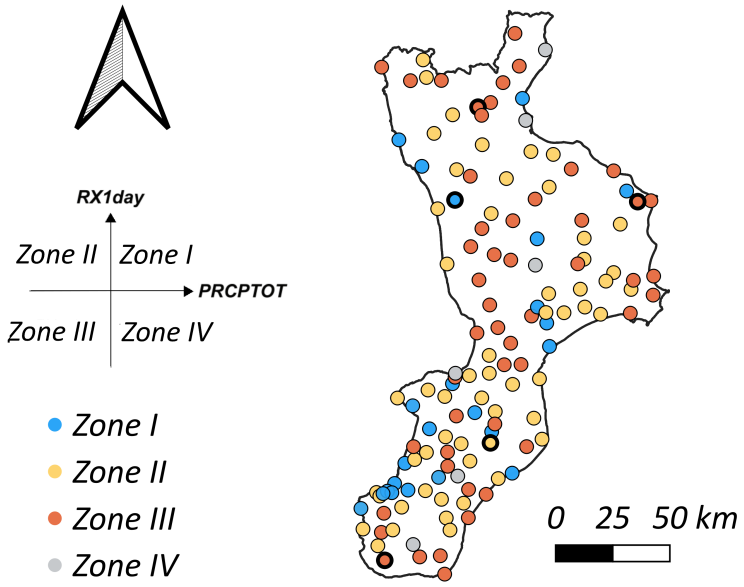

Figure 6. Four zones of compound trends of PRCPTOT and RX1day at the annual scale for observations over Calabria from 1955 to 2023, according to the diagram shown in Fig. 2. Black-contoured dots represent stations where both trends are statistically significant. The quadrant classification diagram is reproduced for the reader's convenience on the left of the Fig..

pixels and stations exhibiting positive or negative trends) is remarkable, with 62.1% and 66.4% for PRCPTOT and RX1day, respectively.

Another evaluation has been made by comparing the four zones that accommodate the compound annual PRCPTOT and RX1day trends over the Calabria region, as illustrated in Fig. S4. This analysis reveals that ERA5-Land mainly represents zones I and II, whereas ground-truth measurements indicate that zones II and III are the majority. In this case, the level of agreement between the ERA5-Land pixels and the overlying stations is 33.6%, primarily due to the matching of pixels and stations in zone II, which, however, is the zone of major interest in this study.

The comparison between the large-scale reanalysis dataset and the local-scale ground observations demonstrates that the ERA5-Land dataset can generally capture the contrasting daily and annual precipitation trends in Calabria. More generally, the analysis, also combined with other studies evaluating observations-based trends at the Mediterranean level (Gomis-Cebolla et al., 2023; Vicente-Serrano et al., 2025; Beranová et al., 2025), highlights that the Calabrian Peninsula shares with a relevant part of the northern Mediterranean Basin the paradox of decreasing mean/increasing variance. Furthermore, it benefits from a dense and reliable monitoring network. These features are particularly helpful for supporting further analysis of climate evolution and related challenges in the study region. Specifically, the following sections will focus on the connection between

extreme events in Calabria and SST since the latter is a critical variable in disentangling the seemingly counterintuitive outcome of increasing RX1day trends in a general context of decreasing PRCPTOT.

3.2 Observed and projected SST warming

Figure 7 shows the evolution of both the observed and projected yearly average SST in the external domain (D01) of the WRF simulation (Fig. 1). The increasing trend is almost monotonic for both observations and projections, whose agreement lies in the expected range (Menemenlis et al., 2025). Concerning observations, a substantially similar difference of approximately 1.3 °C emerges when examining the average values of the first and last five years of both ERA5 and CMEMS datasets. Such a difference, which agrees with previous literature (Mohamed et al., 2019; Pastor et al., 2020; Sannino et al., 2022), is only slightly higher than that found in the period from September to December (1.1 °C), which will be further addressed with the WRF simulations.

Concerning projections, temperature changes were evaluated by comparing the future periods (2040-2069 and 2070-2098) with the reference period (1985-2014) for both SSP scenarios (Fig. 8). At the annual scale, the projected temperature increase for the SSP3-7.0 scenario is, on average, 1.7±0.4 °C (with the term after the symbol "±" being the standard deviation) and 2.8±0.7 °C for the periods 2040-2069 and 2070-2098, respectively. Concerning the SSP5-8.5 scenario, instead, the differences are, on average, equal, for the same periods, to 2.0±0.5 °C and 3.5±0.9 °C, respectively (not far from what was already projected by the CMIP5 models, e.g. Sannino et al. 2022). The differences detected at the annual scale are nearly identical to those found in the period from September to December, as highlighted by an analysis performed at the monthly scale. The values found for this 4-month period are equal to 1.7±0.5 °C and 2.9±0.7 °C for SSP3 and 2.1±0.6 °C and 3.6±0.9 °C for SSP5, considering the 2040-2069 and 2070-2098 period, respectively. In particular, the 3rd quartile in the period 2070-2098 is equal to 3.2 °C with SSP3-7.0 and 4.1 °C with SSP5-8.5.

The period selected for the high-resolution weather simulations was September to December 2019. During that time interval, the average SST recorded was approximately 1.4 °C above the average SST of the first five years for which observations were available, and approximately 0.9 °C higher than in the reference period 1985-2014. Therefore, a homogeneous 1 °C reduction of the SST fields is a reasonable choice to trace back SST average conditions to the early ’80s. In contrast, a homogeneous increase of 3 °C in the SST fields allows for reproducing the warmest projected conditions for both the SSP3-7.0 and the SSP5-8.5 scenarios in the farthest future period, 2070-2098 (Fig. 8). Hereafter, the simulation considering the actual SST conditions will be referred to as SST0, the past scenario with uniformly reduced SST values as SST-1, and the future scenario with uniformly increased SST values as SST+3.

3.3 High-resolution atmospheric simulations

The time sequence of the 20 events identified and labeled during the analyzed season is depicted in Fig. 9, in which the average daily precipitation values obtained for the Calabria region by spatial interpolation of the 150 available gauges are shown.

Model validation using SST0 was performed for all 20 detected events. While Figs. S5-S24 in the Supplementary show the observed and simulated accumulated precipitation maps for all events, Fig. 10 compares the verification indices FSS

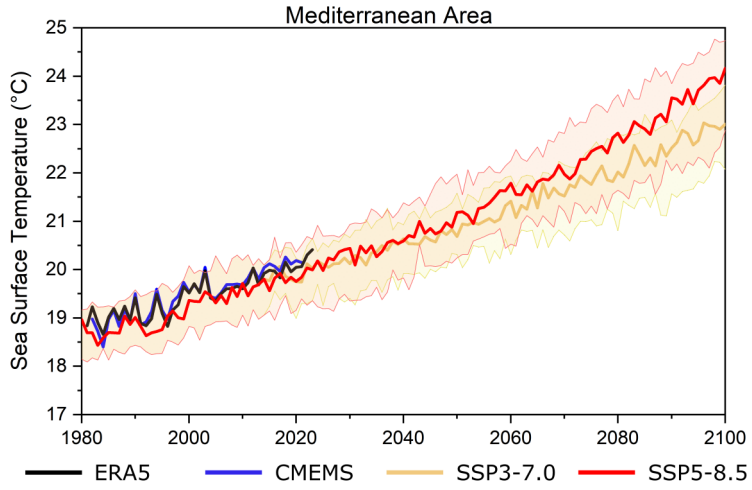

Figure 7. Annual average SST (°C) in the external domain (D01) of the WRF simulation. For SSP3-7.0 and SSP5-8.5 scenarios, the thicker lines indicate the median for the model simulations, while the colored bands highlight the 10th and 90th percentiles, respectively. The area on which the values are calculated is the D01 domain, shown in Fig. 1.

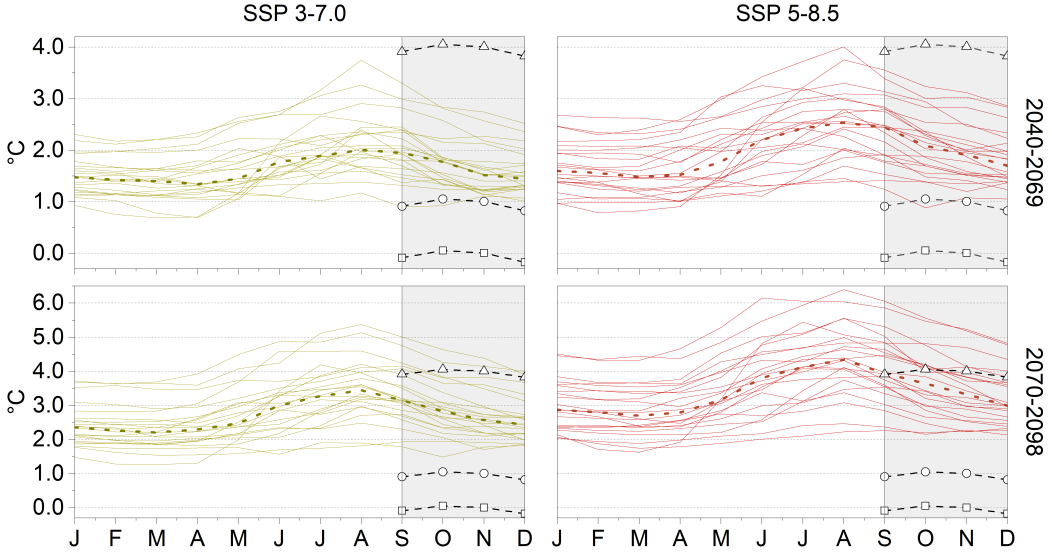

Figure 8. Monthly spaghetti graphs, showing the SST increase compared to 1985-2014 in the periods 2040-2069 and 2070-2098, considering 22 GCMs with both SSP3-7.0 and SSP5-8.5 scenarios, respectively. The dashed lines in each graph represent the medians, and the shaded areas highlight the period from September to December. The dashed lines with circles indicate the observed anomaly in 2019 compared to the reference period, while the triangles and squares represent the changes applied to the observed SST values (+3 °C and -1 °C, respectively). The area on which the values are calculated is the D01 domain, shown in Fig. 1.

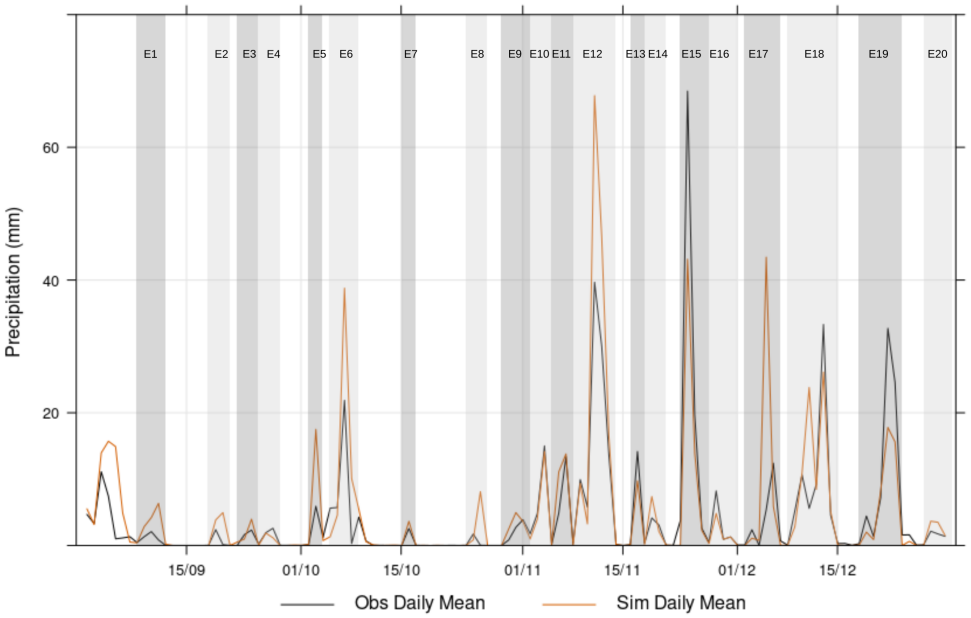

Figure 9. Temporal evolution of daily mean precipitation [mm] for the Calabria region in the analyzed fall 2019 period. The black line represents the observed values obtained through spatial interpolation of observations, and the orange line indicates the results of the SST0 simulation for the same area. In the Fig., each event is identified and labeled.

and CSI achieved for SST0, SST-1, and SST+3 scenarios, as well as the ERA5 reanalysis. Specifically, Fig. 10a illustrates the FSS, highlighting the importance of dynamic downscaling for an accurate representation and demonstrating its superior performance compared to the lower-resolution ERA5. Considering all 20 events, the median FSS increases for larger window sizes as expected, exceeding already for a window size of 3 km the value of 0.5, which is generally considered a benchmark for a skillful forecast, even though a small increase should be taken into account to consider the occurrence of half of a random forecast (Roberts and Lean, 2008; Necker et al., 2024). The FSS is also shown for the SST-1 and SST+3 simulations, with the aim of highlighting the extent to which SST representation affects the simulations. Due to its higher difference from observed SST, SST+3 performance does not increase as much as SST-1 with increasing window size. Still, the SST+3 simulation remains better than the reanalysis. Considering the CSI index (Fig. 10b), all models perform relatively well for smaller precipitation thresholds. In contrast, as the threshold increases, the simulation with SST0 performs the best. It can also be seen that ERA5 has a median of 0 when considering the threshold of 30 mm, indicating that at least 50% of the events have no prediction skill.

After validating the simulations against observational data, we conducted an in-depth analysis of how varying sea surface temperature boundary conditions influence precipitation patterns. Considering the whole innermost domain at convection-permitting resolution (D02 in Fig. 1b), precipitation increases as the SST increases. In fact, the simulated accumulated precipitations for the 20 events analyzed are always lower for the past scenario (SST-1) and higher for the future scenario (SST+3) than

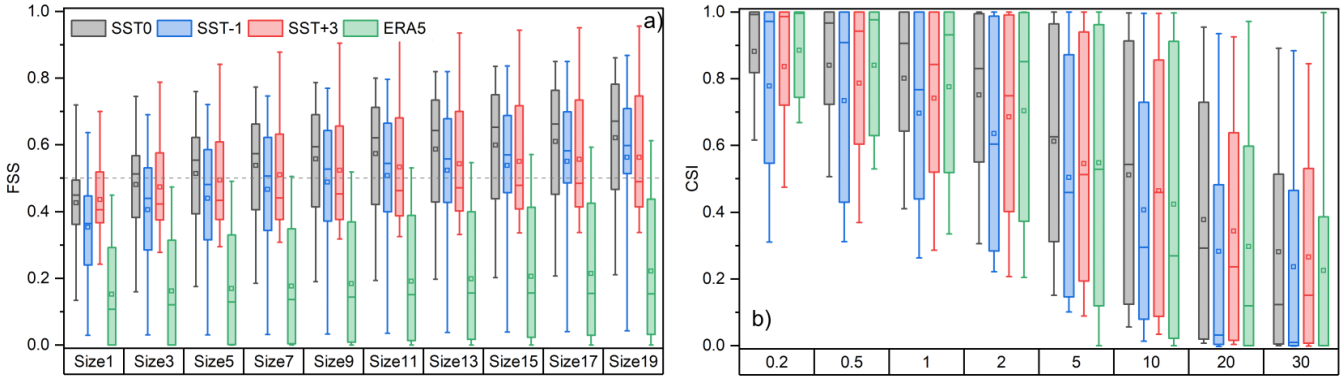

Figure 10. Box and whisker plots of the Fractional Skill Score (a) and the Critical Success Index (b) obtained by considering all the identified precipitation events and the three SST scenarios over the Calabria region. Each boxplot represents the variability across the 20 different events. The size in the FSS sub-figure indicates the size of the moving average windows, as specified in Eq. 1. Conversely, in the CSI sub-figure, the label indicates the precipitation threshold (mm). In the boxplots, the bottom and up whiskers indicate the 5th and 95th percentiles, respectively; the box limits the 1st and the 3rd quartiles, respectively, and the small line in the box is the median. The squares represent the average values.

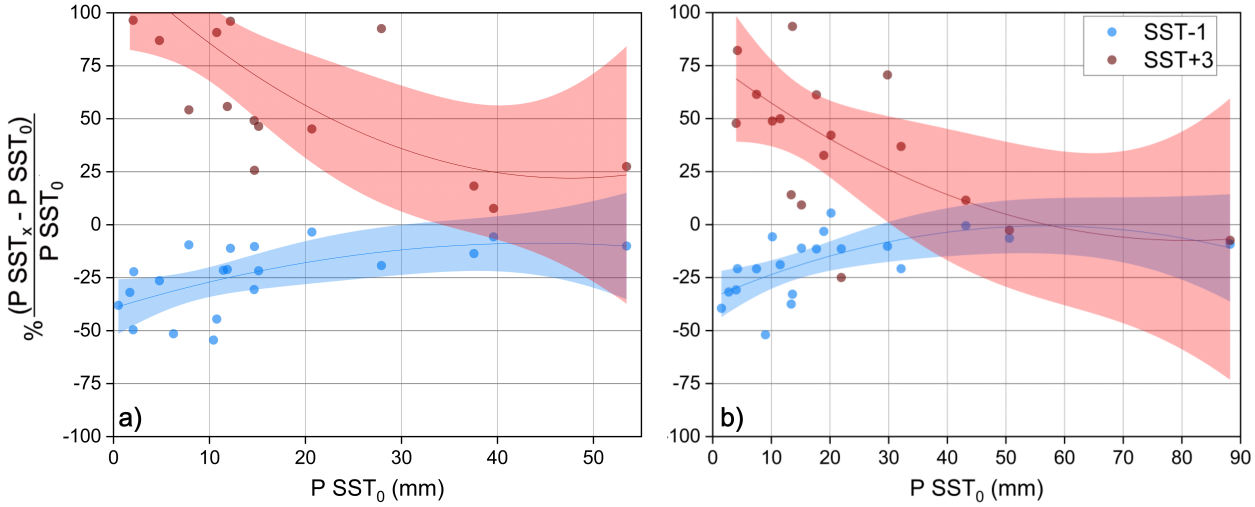

Figure 11. Percentage variation of the accumulated (spatially-averaged) precipitation all over the D02 domain (a) and only overland (b) for each event with SST-1 (blue dots) and SST+3 (red dots) boundary conditions vs. accumulated overland precipitation with SST0 boundary conditions. The shaded areas represent the 95th percentile confidence level performed for the 2nd-order polynomial fitting (represented with the lines) over the two different scenarios.

the actual conditions (SST0), as shown in Table A1 in the Appendix and in Fig. 11a, which sets out the percentage of difference in precipitation between simulations using modified boundary conditions and the SST0 boundary condition compared to the

accumulated precipitation simulated with SST0. This outcome indicates that higher precipitation occurs when a greater amount of water vapor is available in the atmosphere, due to a larger contribution of evaporation from a warmer sea. Specifically, the precipitation amounts (spatial average) collected for all events with different SSTs are quite well linearly correlated so that it is $P_{SST-1} = 0.92 \cdot P_{SST0} - 1.4$ ($r = 0.99$) and $P_{SST+3} = 1.14 \cdot P_{SST0} + 6.4$ ($r = 0.95$), with P_{SSTx} [mm] indicating the accumulated precipitation with the given SST boundary condition.

If only accumulated rainfall on land is considered rather than over the whole domain D02 (Table A1 and Fig. 11b), the linear correlations between P_{SST0} and P_{SST-1} and P_{SST+3} still hold, being $P_{SST-1} = 0.94 \cdot P_{SST0} - 1.1$ ($r = 0.99$) and $P_{SST+3} = 0.88 \cdot P_{SST0} + 8.5$ ($r = 0.94$), respectively. Nevertheless, the increase in precipitation in response to SST increase is no longer always respected, especially for higher precipitation, as the slopes of the linear equations (higher for P_{SST-1} in this case) suggest. Opposite trends arise considering SST-1 and SST+3. In the case of low SST0 precipitation values (i.e., light events), colder SST conditions lead to markedly reduced rainfall (approximately from -25% to -50%). In comparison, warmer SST conditions produce the opposite effect, with increases up to +75% and even more. However, when accumulated precipitation values with SST0 increase (i.e., in the case of heavier events), both the colder/warmer SST-induced precipitation differences tend to cancel out. For the two heavier events, the precipitation differences for SST-1 are equal to -6% and -9%, while for SST+3, they are equal to -3% and -7%, respectively.

The counterintuitive behavior of overland accumulated rainfall, which, for the heavier events, tends to decrease despite the higher SST values, is linked to the changes in the spatial pattern of the precipitation fields in the domain and, in particular, to the eastward shift of the rainfall peaks. Figure 12 depicts with circles the locations of the barycenters of the precipitation patterns calculated as described in section 2.4. In the Fig., the circles related to the same event but with different SST boundary conditions are connected by blue (SST-1 to SST0 barycenters) and red (SST0 to SST+3 barycenters) lines, and the small arrows indicate the predominant wind directions at 850 hPa during the events. For each triplet, the size of the red circle, representing the average precipitation of the pixels exceeding the 95th percentile for that event, is always bigger than the sizes of the blue (SST-1) and grey (SST0) circles. Indeed, such as for average precipitation, also rainfall peaks (Table A1) are linearly correlated ($P_{SST-1} = 0.88 \cdot P_{SST0} - 1.6$ with $r = 0.98$ and $P_{SST+3} = 1.13 \cdot P_{SST0} + 28.6$ with $r = 0.92$, respectively).

Besides the amount of rainfall peaks, however, for our purposes, their different locations are particularly important. Figure 12 highlights that in most cases, the increased rainfall peaks of the SST+3 events are shifted eastwards of the respective SST0 events. Some of them, notably the rainiest events (nos. 6 and 12), are relocated over the Ionian Sea, thereby saving the land from the heaviest rainfall. Such an effect was found especially for the cyclonic circulations that cross the Ionian Sea before reaching the eastern Calabrian coast, which are, in general, the heaviest and most impactful. The warmer boundary conditions modify appreciably the circulation pattern (for example, for event no. 12, the blue circle is over the Tyrrhenian Sea and the red one over the Ionian Sea) and, mainly, foster the upload of significant moisture content from the sea, enhancing instability so that the heaviest precipitation is induced offshore rather than overland. Notably, this behavior is also caught with lower-resolution simulations (Fig. S25 shows the same analysis of Fig. 12 performed using the external domain). In addition, sensitivity analyses highlighted that the eastward shifting is quite a robust outcome, not depending on the atmospheric model

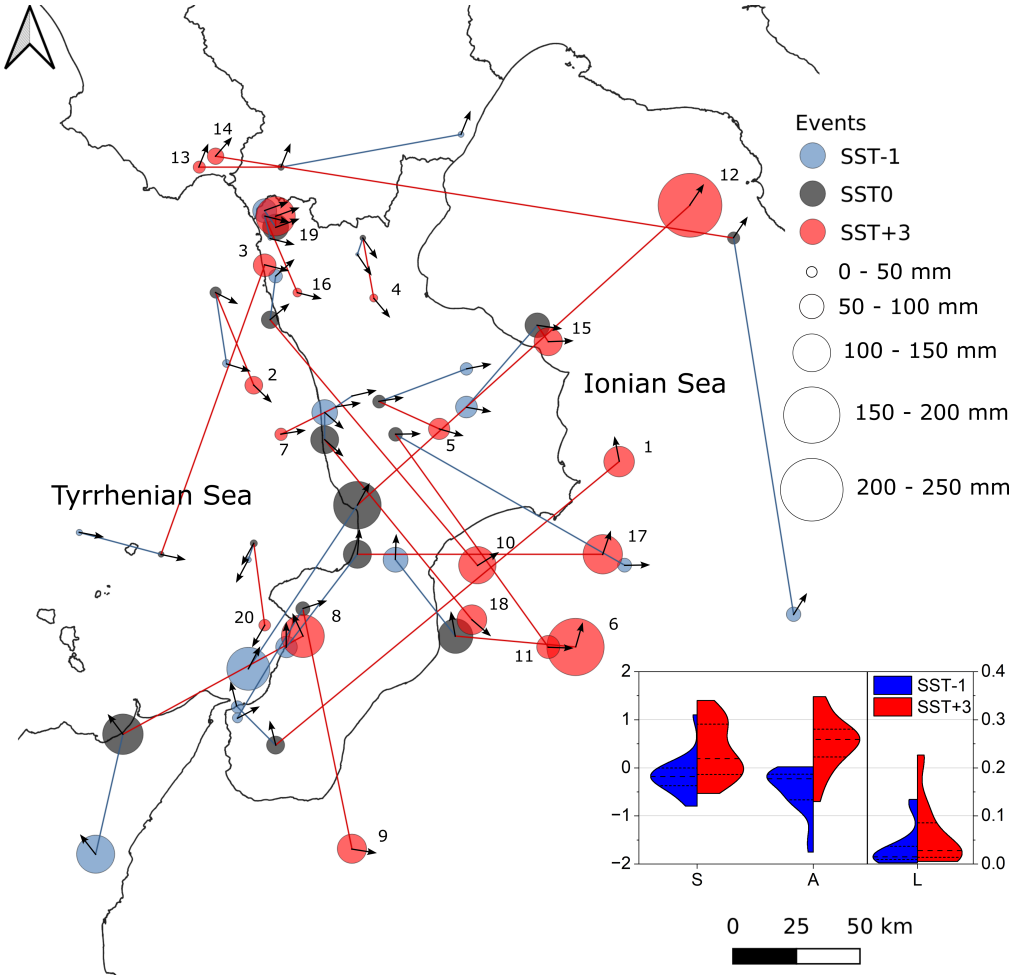

Figure 12. Locations of the centers of mass of the accumulated precipitation exceeding the 95th percentile for the 20 analyzed events, considering the innermost domain, with SST-1 (blue filled circles), SST0 (dark grey), and SST+3 (red). The small arrows indicate the predominant wind directions at 850 hPa during the events, calculated as the average values over the whole D02 domain. The inset shows the SAL violin plot by considering the SST-1 and SST+3 scenarios with respect to SST0; the dashed line indicates the median, while the dotted lines highlight the 1st and 3rd quartiles, respectively.

parameterization (Fig. S26 shows that using a different PBL scheme, i.e., YSU - Yonsei University scheme, Hong et al. 2006, does not cause substantial changes in SST0 and SST+3 precipitation patterns for event no. 12).

The eastward shift is caused by changes in cyclone structure induced by warmer sea-surface temperatures (SSTs). Higher SSTs increase the energy and moisture available to storms, producing deeper, larger cyclones with stronger winds. As a result, the cyclone precipitation footprint — which generally lies east–northeast of the pressure minimum (e.g., Field and Wood 2007) — becomes larger and extends further east/northeast. This scaling also applies to the synoptic patterns most responsible for intense precipitation over the Calabrian peninsula, whose lows often center over a region including the Strait of Sicily

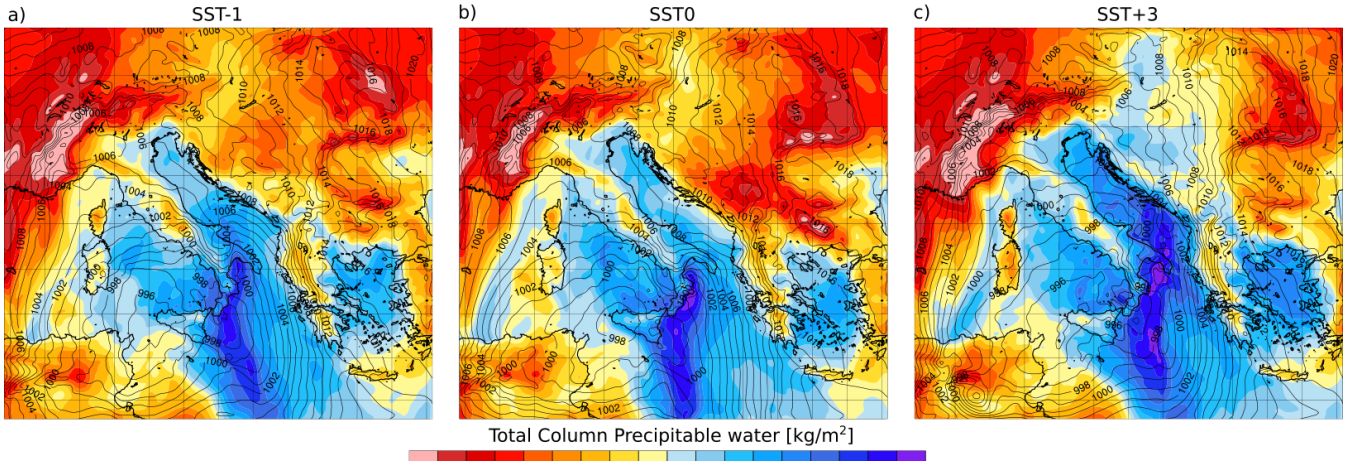

Figure 13. Column precipitable water (kg m^{-2}) for configurations a) SST-1, b) SST0 and c) SST+3 on 12 November 2019 at 03:00 GMT. The maps also show sea level pressure (contours; hPa).

and the Tyrrhenian Sea (e.g., Mastrantonas et al. 2022). Thus, SST-driven increases in cyclone size can relocate the heaviest precipitation from overland (where, however, orographic enhancement is possible) to offshore areas in the Ionian Sea.

The SAL analysis, shown in the inset of Fig. 12, objectively confirms the visual analysis. The SST-1 scenario mainly generates negative S and A components, thus smoothing and reducing the precipitation fields. On the other hand, the SST+3 scenario tends to be sharper and to increase the average precipitation. The L component, which in principle can vary from 0 to 2, depicts a more prominent increase in distance between the centres of mass when applying SST+3 compared to SST-1.

Event no. 12, which produced the heaviest simulated precipitation, was analyzed in detail as an exemplary case to better explain the dynamics leading to the eastward shift of the precipitation maxima. Figure 13 shows a snapshot of the large-scale pattern during the event. As described above, the cyclone dominating the western Mediterranean Basin, though being in all cases broadly centered on west Sicily, is deeper and larger with SST+3 than with SST0 and SST-1, increasing the amount of precipitable water in the atmosphere and moving eastward the barycenter of the water vapor concentration pattern. The characteristics of event no. 12 are also reflected in the large-scale analysis of other events, namely nos. 6 and 15, as shown in Fig. S27, with the differences that for event no. 6 the pressure low is centered southward, closer to the Libyan coast, and for event no. 15 in the central Tyrrhenian Sea.

Focusing on higher-resolution simulations (domain D02) of event no. 12, Fig. 14 shows the average convective available potential energy (CAPE) during the night preceding the most intense rainfall (Figs. 14a, c, and e), together with the average water vapor mixing ratio, vertical wind and vertical velocity omega profiles (Figs. 14b, d, and f) for a specific cross-section (red line in Figs. 14a, c, and e). The experiment produced a substantial increase in CAPE on the Ionian Sea as SST increased, indicating a more considerable offshore instability for this kind of event in future scenarios. The vertical profile of omega, water vapor mixing ratio, and vertical wind at the selected cross-section confirmed this result. Negative values of omega describe

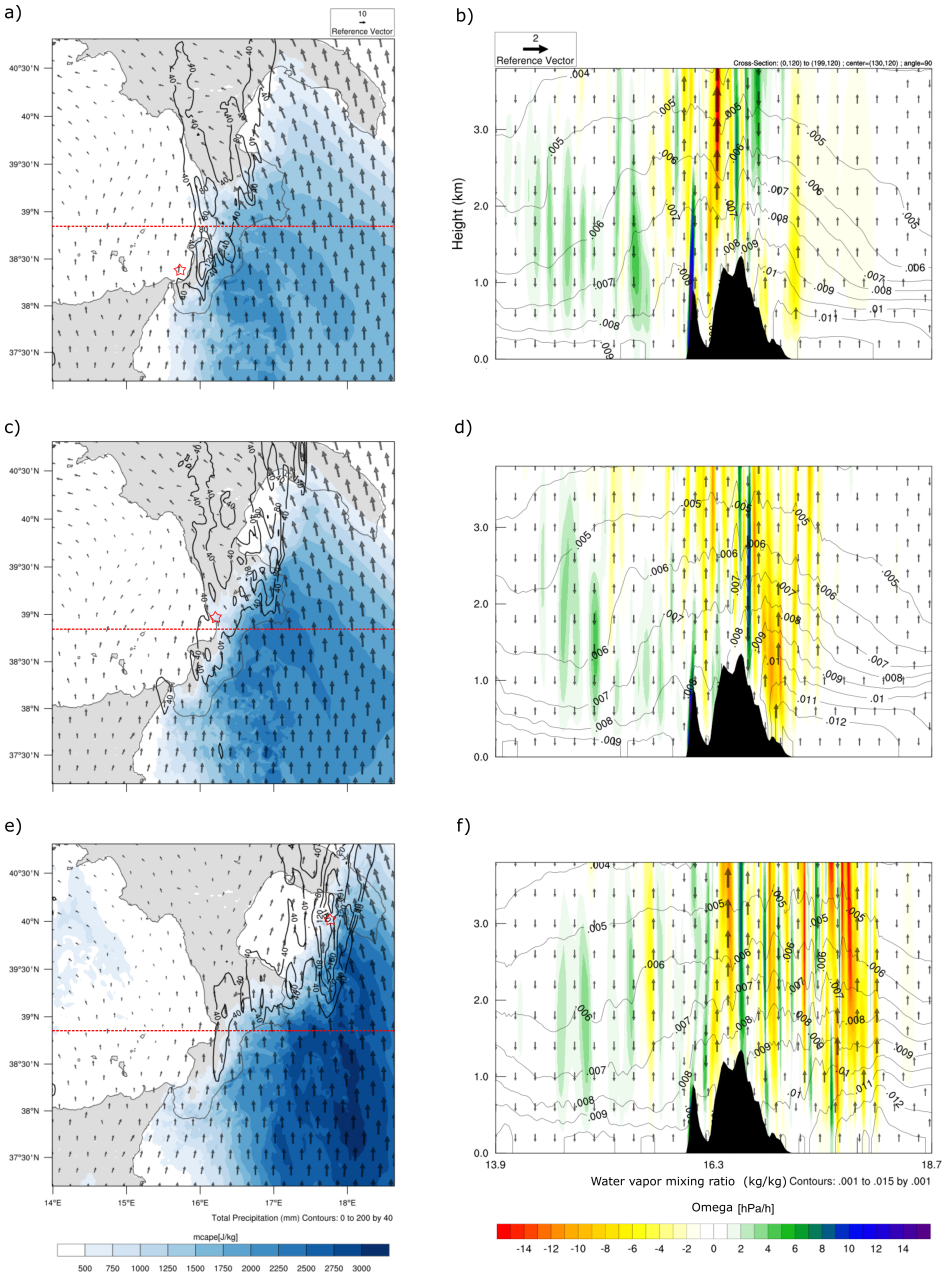

Figure 14. Left: Average CAPE (color bar), horizontal average wind at 850 hpa (arrows), and precipitation (isolines) during the eight hours preceding the most intense rainfall during event no. 12: a) SST-1, c) SST0, e) SST+3. The red star indicates the center of mass previously shown in Fig. 12. Right: vertical profile of omega (color bar), water vapor mixing ratio (isolines), and vertical wind (upward or downward arrows for direction; speed proportional to the reference vector) for b) SST-1, d) SST0, f) SST+3.

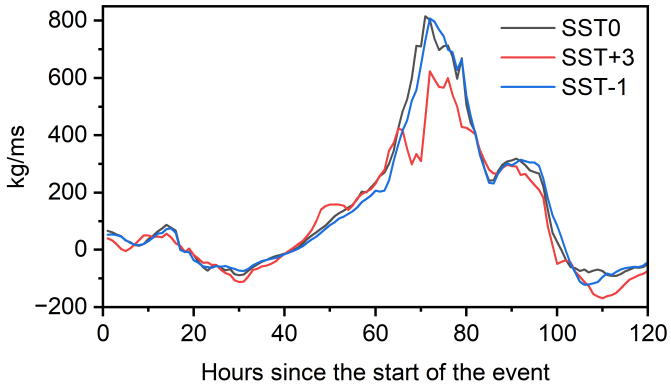

Figure 15. Temporal evolution of the vertically integrated water vapor flux (kg/ms), perpendicular to section A-A' shown in Fig. 1a, during event 12.

unstable conditions, which were shifted eastwards with increasing SST. Additionally, the specific humidity in the atmosphere increased over the Ionian Sea, and the ascending currents were stronger. Therefore, Fig. 14 underscores that the atmospheric instability and the moisture content can be shifted eastwards and offshore while moving towards warmer SST conditions. The same analysis, performed for events no. 6 (Fig. S28) and 15 (Fig. S29), showed similar outcomes, even though the difference in the vertical profile of omega in the latter case, having a minimal eastward shift, is less marked.

Finally, still focusing on event no. 12, another effect of the SST scenario selection is shown in Fig. 15, with the column-integrated water vapor flux crossing the section A-A' shown in Fig. 1a. The analysis indicates that the SST+3 scenario reduced the overall amount of water vapor flowing towards the eastern coast of Calabria by almost -24 %. According to previous analyses, with the SST+3 simulation, the water vapor mainly flows northward, approximately parallel to the coastline, until it triggers intense rainfall.

4 Discussion

4.1 Trend analysis

The reliability of the trend analysis at the large scale strongly depends on the ability of ERA5-Land to capture the contrasting daily and annual precipitation trends. Our findings make further contributions to the existing literature on the soundness of trend reconstruction using ERA5 and ERA5-Land, particularly along the northern Mediterranean coast. The analysis performed over Calabria highlights that the ERA5-Land dataset provides more smoothed precipitation time series in comparison with the gauges, which take more localized variations (not necessarily representative of an entire ERA5-Land grid cell); a conclusion strongly supported by Gomis-Cebolla et al. (2023) implying underestimations of ERA5/ERA5-Land for heavy (from 20 to 40 mm/day) and violent precipitation (exceeding 40 mm/day) categories over Spain apart from their good capacity to introduce

the spatial patterns and temporal trends of observations from 1951 to 2020, by Beranová et al. (2025), concluding the tendency of reanalyses like ERA5 to underestimate total precipitation in wintertime over Europe considering observations from 1961 to 2010, and by Cammalleri et al. (2024), finding that ERA5 captures inter-annual variability trends in Southern Italy. Being based on a reanalysis, the ERA5-Land dataset relies on observations indirectly, providing a spatially homogeneous level of accuracy. Other spatially distributed datasets directly based on ground data supply biased information in zones where the monitoring network is not dense enough. For example, the stations feeding the E-OBS dataset (Cornes et al., 2018) are rather sparse in southern and eastern Europe (Cammalleri et al., 2024). Also, concerning the hydrological impact, the findings of Stahl et al. (2012) and Blöschl et al. (2019) about decreasing regional trends of river flood discharges in southern Europe are contradicted by Prete et al. (2023) and Avino et al. (2024) local-scale findings about daily precipitation trends, probably because in the studies analyzing streamflow data very sparse observations are available for this region. Finally, a recent study based on a comprehensive station-based dataset for the whole Mediterranean region (Vicente-Serrano et al., 2025) confirms a general decreasing trend for annual precipitation in the period 1951-2020, attributing it to internal variability of atmospheric dynamics.

Despite the inevitable uncertainty that accompanies the use of any large-scale grid dataset, trend results in the Mediterranean are largely consistent with the previous literature and support the mentioned paradox of decreasing mean/increasing variance. Summarizing several previous studies, also the 6th IPCC Assessment Report (Masson-Delmotte et al., 2021) highlights significantly increased observed heavy precipitation in northern and central Europe and a lower agreement in the type of change for the Mediterranean area. In contrast, a significant increase was observed in agricultural and ecological drought in the Mediterranean and Western and Central Europe, with low agreement for the trend sign in other European areas. Similarly, results concerning Calabrian gauges' trends reveal consistent outcomes with those of previous studies. In particular, Prete et al. (2023) found increasing daily rainfall extremes for 50- and 100-year return periods, Avino et al. (2024) pointed out generally increasing trends for daily and sub-daily rainfall durations, and Caloiero et al. (2020, 2021) observed a decreasing trend in annual rainfall. On the contrary, Caloiero et al. (2017) asserted a decreasing trend in the higher daily rainfall categories, but with a dataset that stopped in 2006.

However, an important point to consider for both the analyzed datasets is that, while the pattern of the spatial distributions of both PRCPTOT and RX1day trends is clear, with the prevalence of decreasing PRCPTOT and increasing RX1day, many of the detected trends are statistically non-significant, especially concerning RX1day. There are multiple possible reasons for this outcome. Of course, the simplest is that the trend signal in the time series is too weak. However, the statistically non-significant trends observed in ERA5-Land may also stem from issues related to spatial aggregation (Guo et al., 2024), potentially smoothing out localized variations and extreme events captured by ground observations, and model biases (Xie et al., 2022), arising from assumptions made in the simulation of physical processes. Regarding point-based precipitation measurements, the issue of statistically nonsignificant trends may originate from recurrent outliers (González-Rouco et al., 2001), which can be attributed to instrument malfunctions and environmental influences such as wind. In our dataset, although outliers in a few cases contributed to the loss of statistical significance, they were not removed, as they were considered verified observations.

4.2 Mediterranean Sea warming effect on precipitation

To the best of the authors' knowledge, this research, for the first time, aims at disentangling the expected influence of sea surface warming, even combined with orography, on cyclonic event features in Southern Europe, by analyzing an entire season with 20 events at a convection-permitting resolution, and highlighting variations in features like average and maximum accumulation precipitation values and overall spatial patterns. Our experiments extend and are directly comparable to the existing body of literature focusing on the Mediterranean area. Meredith et al. (2015), analysing a single Black Sea event at very high resolution, chiefly reported a large increase in simulated precipitation and also substantial changes in the rainfall patterns. By contrast, studies that considered multiple events in the Adriatic (Stocchi and Davolio, 2017; Ricchi et al., 2023) emphasised that the effect of SST varies considerably between events and that SST mainly influences the stability of the atmospheric boundary layer. Focusing on Medicanes, Fita et al. (2007) and Miglietta et al. (2011) showed that warming or cooling of the sea surface can affect Medicane formation, producing much more intense and larger systems with higher SST; Pytharoulis (2018) found an almost linear deepening of Medicanes with increasing SST anomalies and noted that Medicane lifetime depends on SST. Noyelle et al. (2019), while agreeing on the strong SST influence on Medicane intensity, concluded that the SST state has only a minor effect on cyclone tracks. Conversely, Varlas et al. (2023) attributed both the intensity and the track and landfall location of the Ianos Medicane to SST changes. In other world regions, Lin et al. (2023) argued that SST modifies the marine boundary-layer jet, which can shift Taiwanese rainfall southward, whereas Dutheil et al. (2019) found that rainfall variations in the South Pacific Convergence Zone are driven by uncertain changes in the zonal SST gradient consistent with a "warmer-gets-wetter" mechanism. Finally, Armon et al. (2022), analysing many historical events, reported a substantial decrease in rainfall accumulation in the eastern Mediterranean, caused by a marked reduction in storm rain area and shorter storm duration, even though mean conditional rain intensity increased.

While this research expressly focuses on SST warming trajectories, to achieve a more comprehensive overview of future conditions, other information should be complemented. For example, contrary to the pseudo-global warming approach used here, generally, the atmosphere's vertical profile is also expected to be modified. Varying only SST can lead to an overestimate in the vertical gradient of temperature and, therefore, biased effects on precipitation. The present analysis treats each event individually and regards them as isolated phenomena, such as, e.g., the cold air intrusions that typically occur in this area at this time of year, and are therefore plausible also in a global warming scenario, not undermining the relevance of our experiments. Nevertheless, changes in event frequency or seasonality cannot be assessed with our event-based, SST-only framework. Important forcings and feedbacks are omitted, such as, for example, the effects of increased salinity levels due to lower precipitation and freshwater supply (Verri et al., 2024), which could lead to reduced evaporation and consequently less severe precipitation events (e.g., Lee and Hong 2019). Coupled GCM/RCM scenarios, on the other hand, account for multiple drivers simultaneously and can produce additional effects such as a shortened rainy season (Hochman et al., 2018), weakened land–sea thermal contrasts (Tuel and Eltahir, 2020), and altered cyclone frequency and tracks through changes in large-scale circulation. However, although much recent literature relying on GCM- and RCM-based scenarios focuses on the projection of heavy rainfall events in the central Mediterranean, it does not yet provide a unanimous response.

Analyzing the decomposed contribution from atmospheric thermodynamics and dynamics in CMIP5 projections, Pfahl et al. (2017) concluded that reduced cyclone frequency is expected in the broader Mediterranean region. Both Zappa et al. (2015), analyzing 17 CMIP climate models, and Reale et al. (2022), considering a higher resolution provided by the Med-CORDEX (CMIP5-derived) ensemble, for the end of this century found that the overall frequency decrease and weakening of cyclones moving across the Mediterranean will be compensated, in the central part, by increased wind speed and precipitation rate. Using the EURO-CORDEX ensemble, Matte et al. (2022) projected for the Central Mediterranean an increase in the number of events exceeding the 90th percentile for the larger-sized precipitation systems and a small decrease for medium-sized systems. Also, Hosseinzadehtalaei et al. (2020), projecting intensity–duration–frequency curves over Europe, showed that the sub-daily extreme precipitation events with the highest return periods are expected to become more frequent. Another analysis based on the EURO-CORDEX ensemble and focused on precipitation overland (Tramblay and Somot, 2018) emphasizes an overall increase in 20-year extreme precipitation in the northern Mediterranean coast and a decrease in the southern coast, in agreement with the ongoing trends described in this paper (section 3.1). Finally, by further increasing the spatial resolution with an ensemble of convection-permitting regional climate models under the RCP8.5 forcing scenario, Müller et al. (2024) found that more intense, heavy, and severe precipitation events must be expected in southern Italy, especially during fall in the form of landfalling and geographically forced events. Moving to CMIP6 projections, Fernández-Alvarez et al. (2023), analyzing the Community Earth System Model Version 2 (CESM2; Danabasoglu 2023) under the SSP5-8.5 scenario, recognized a contrasting contribution of moisture transport from the Mediterranean Sea and the North Atlantic Ocean to the western continental area of the Mediterranean basin, with the former increasing precipitation and the latter decreasing it. Finally, Anav et al. (2024) performed a dynamical downscaling of the MPI-ESM1-2-HR model (model no. 18 in Table 1). Concerning precipitation, they only provided results at the seasonal scale, revealing a substantial reduction. However, they demonstrated that the high-resolution air-sea coupling improved the representation of high-impact events like marine heat waves.

In the overview of heavy rainfall projections summarized above, the risk of high-impact events increases, in general, with increasing resolution of the simulation. This outcome can be explained by considering the more relevant effect of higher-resolution complex topography in triggering convection (Ricchi et al., 2023). Using very high-resolution (2 km) modeling, our study demonstrated that the interaction of an increasingly warmer and humid atmosphere with coastal orography, which impacts the development of convective systems even offshore (Khodayar et al., 2021), further enhances the moisture loading and favors their maturity so that rainfall peaks occur before landfall, especially for more unstable systems. In this way, given a precipitation rate increase in the overall domain (i.e., considering both land and sea), the overland precipitation rate increases for small to medium-sized events, making them more dangerous and impactful, but is constant or even reduces slightly for heavy events, which, however, remain still dangerous. Therefore, the overall tendency overland can be summarized as an expected increasing frequency of heavy events rather than increasing intensity.

5 Summary and conclusions

The research provides an investigation of the decreasing mean/increasing variance paradox of precipitation in southern Europe. First, a combined trend analysis of annual and maximum one-day precipitation over the Mediterranean region revealed divergent trends along much of Southern Europe, with heavy precipitation increasing but total annual precipitation decreasing. These trends were compared with those achieved by ground-based measurements in the Calabrian peninsula, leveraging an observational dataset spanning nearly 70 years. The results confirmed the general reliability of the ERA5-Land dataset and pointed out that this subregion can be considered representative of much of the northern Mediterranean coast.

Next, we examined the role of sea-atmosphere-orography interactions in explaining heavy precipitation enhancement despite the overall drying trend. In particular, we isolated the impact of sea surface warming by simulating an especially intense rainy season in the Calabrian peninsula and comparing current SST conditions with both past (SST-1) and future (SST+3) scenarios. The convection-permitting resolution of the dynamical downscaling approach allowed for a highly detailed reconstruction of the different cyclone features and the resulting precipitation patterns induced by varying SST boundary conditions. The numerical experiments explained the enhancement of overland heavy precipitation events' frequency but did not indicate an increase in peak rainfall accumulation since the most extreme events should tend to produce their highest rainfall totals over the sea before reaching land.

The study's main methodological contribution is demonstrating the added value of high-resolution, convection-permitting analyses in accurately capturing key processes unique in orographically complex regions like the one addressed. The benefit of such an approach has been highlighted by several different studies in the past (e.g., Ban et al. 2014; Prein et al. 2015; Coppola et al. 2020; Pichelli et al. 2021), but its advantages continue to be thoroughly evaluated even in more recent studies (e.g., Fosser et al. 2024; Soares et al. 2024). While we showed that the main features of precipitation change can be observed already by examining the outer (lower resolution) domain, the approach adopted helps explain in detail the seemingly contradictory trends of increasing daily maximum rainfall and decreasing annual total precipitation, and can be generalized to much of the northern Mediterranean coast. As hyper-resolution climate simulations become more widely available, they will allow for further validation and refinement of these results.

Overall, our results help clarify the specific role of Mediterranean Sea warming in shaping the evolution of precipitation regimes in the study area. This work advances previous findings by preliminarily updating the analysis of current trends with the most recent data available and then by systematically examining the effects of predicted SST increase over an entire rainy season. In doing so, it highlights changes not only in precipitation accumulation but also in its spatial distribution, including minor events. The findings reveal a distinctive situation characteristic of the central–western Mediterranean domain, which contrasts with other zones of the basin (i.e., the eastern Mediterranean; Armon et al. 2022), where synoptic circulation causes the sea to contribute differently as a reservoir of atmospheric moisture for projected storms.

The focus on overland precipitation underscores the practical implications of this study. As a general indication, the results achieved so far suggest that in the future, rather than the maximum intensity of heavy events, their return period will more probably change. The projected higher frequency of moderate-to-heavy events is a key factor to consider for climate adap-

tation and territorial and urban planning, especially in terms of how extreme precipitation affects flood risk. Of course, this indication needs to be complemented by further analysis, which will be performed in future research. A key focus will be the quantification of the hydrological impact, as the expected rise in heavy precipitation event frequency could disproportionately elevate flood risk, but in different ways, according to the diverse features and sizes of the affected watersheds. The atmospheric modeling performed so far needs to be linked to detailed hydrological modeling to quantify changes in runoff, peak flows, and inundation patterns. Finally, robust assessment requires quantifying uncertainty through multi-experiment ensembles. To this aim, the overall atmospheric-hydrological chain shall be supported by multiple pseudo-global-warming runs and GCM/RCM-driven simulations that account for warming-induced processes beyond SST changes, characterized by sufficiently high (convective-permitting) resolution so that convective processes are explicitly resolved and orographic enhancement effect is duly considered.

Data availability. The daily precipitation at the high resolution simulated by the WRF model in the innermost domain D02 can be downloaded at https://doi.org/10.5281/zenodo.16356046 for all three SST scenarios. Precipitation gauges data are available upon request from the Centro Funzionale Multirischi – ARPACAL (2025; http://www.cfd.calabria.it/index.php/dati-stazioni/dati-storici). ERA5-Land can be retrieved from https://cds.climate.copernicus.eu/datasets/reanalysis-era5-land. ERA5 Data can be retrieved from https://cds.climate.copernicus.eu/datasets/reanalysis-era5-single-levels-monthly-means?tab=overview. CMIP6 Data can be retrieved from https://doi.org/10.20350/digitalCSIC/15492. CMEMS Data can be retrieved from https://doi.org/10.48670/moi-00169.

Appendix A

Table A1 provides a detailed analysis of the 20 precipitation events identified in the September-December 2019 period. It quantifies average precipitation (mm) across the entire internal domain of the WRF simulation, overland-only precipitation, and precipitation above the 95th percentile, simulated by SST0, SST-1, and SST+3 scenarios, respectively.

ID	Start - End Date	n° days	$\bar{P}$ D02 SST0	$\bar{P}$ D02 SST-1	$\bar{P}$ D02 SST+3	$\bar{P}$ Land SST0	$\bar{P}$ land SST-1	$\bar{P}$ land SST+3	$\bar{P} > 95^{th}$ SST0	$\bar{P} > 95^{th}$ SST-1	$\bar{P} > 95^{th}$ SST+3
1	09/09-11/09	3	10.4	4.7	23.8	13.6	9.1	26.3	71.7	48.9	121.9
2	19/09-20/09	2	6.2	3.0	14.2	13.4	8.4	15.3	45.1	31.7	70.8
3	23/09-24/09	2	2.1	1.6	12.4	2.7	1.9	19.3	23.9	25.1	90.7
4	26/09-27/09	2	2.0	1.0	4.0	4.0	2.8	5.9	23.2	13.9	32.1
5	03/10-03/10	1	14.7	13.2	18.4	15.1	13.4	16.5	51.7	49.9	84.9
6	05/10-09/10	5	27.9	22.5	53.7	32.1	25.4	43.9	138.0	99.4	228.1
7	16/10-16/10	1	0.5	0.3	5.5	1.5	0.9	7.2	8.6	5.4	49.5
8	25/10-26/10	2	15.1	11.8	22.1	20.2	21.3	28.7	161.1	151.6	170.7
9	30/10-01/11	3	10.7	6.0	20.5	11.5	9.3	17.2	56.4	40.1	116.5
10	02/11-04/11	3	11.4	9.0	26.4	17.7	15.6	28.5	69.7	54.0	148.6
11	06/11-07/11	2	20.7	19.9	30.0	18.9	18.3	25.1	54.8	55.5	91.9
12	09/11-13/11	5	53.4	48.1	68.1	88.2	80.1	81.7	189.2	170.9	254.1
13	17/11-17/11	1	7.8	7.1	12.1	10.2	9.6	15.1	26.0	23.8	48.5
14	19/11-20/11	2	11.9	9.4	18.5	9.0	4.3	19.4	48.8	57.5	65.6
15	24/11-26/11	3	39.6	37.3	42.6	43.1	42.9	48.1	98.2	86.5	112.7
16	28/11-30/11	3	1.7	1.2	4.0	4.2	3.3	7.7	23.3	18.2	35.7
17	03/12-06/12	4	14.6	10.2	21.9	21.9	19.4	16.4	111.8	85.7	156.7
18	09/12-14/12	6	37.5	32.4	44.4	50.6	47.3	49.3	111.3	102.3	118.6
19	19/12-23/12	5	12.2	10.8	23.9	29.8	26.8	50.8	103.5	95.2	156.8
20	28/12-30/12	3	4.8	3.5	8.9	7.5	5.9	12.0	28.6	23.6	46.5

Table A1. Main features of the events identified in the analyzed period: event ID; starting and ending dates; duration in number of days; average precipitation $\bar{P}$ in the innermost D02 domain simulated by SST0, SST-1, and SST+3 scenarios, respectively; average overland precipitation $\bar{P}$ simulated by SST0, SST-1, and SST+3 scenarios, respectively; average of the accumulated precipitation $\bar{P}$ exceeding the 95th percentile simulated by SST0, SST-1, and SST+3 scenarios, respectively. All values are expressed in mm.

Author contributions. Conceptualization: A.S., G.M.; Data curation: L.F., G.N., Formal analysis: all authors; Investigation: all authors; Methodology: L.F., G.N., J.C., with support of A.S. and G.M.; Software: L.F., G.N.; Supervision: G.M.; Visualization: L.F., G.N., Writing – original draft: A.S. with support of all authors; Writing – review & editing: all authors.

Competing interests. The authors declare that they have no conflict of interest.

Acknowledgements. This work was funded by the Next Generation EU - Italian NRRP, Mission 4, Component 2, Investment 1.5, call for the creation and strengthening of 'Innovation Ecosystems', building 'Territorial R&D Leaders' (Directorial Decree n. 2021/3277) - project Tech4You - Technologies for climate change adaptation and quality of life improvement, n. ECS0000009. This work reflects only the authors' views and opinions, neither the Ministry for University and Research nor the European Commission can be considered responsible for them. We thank the "Centro Funzionale Multirischi" of the Calabrian Regional Agency for the Protection of the Environment for providing the observed precipitation data. Finally, the authors thank Dr. Francesco Leonetti, Dr. Francesco Greco, and Dr. Fabio Cortale for their support in preparing the revised figures.

References

Aguilar, E., Peterson, T. C., Obando, P. R., Frutos, R., Retana, J. A., Solera, M., Soley, J., García, I. G., Araujo, R. M., Santos, A. R., Valle, V. E., Brunet, M., Aguilar, L., Álvarez, L., Bautista, M., Castañón, C., Herrera, L., Ruano, E., Sinay, J. J., Sánchez, E., Oviedo, G. I. H., Obed, F., Salgado, J. E., Vázquez, J. L., Baca, M., Gutiérrez, M., Centella, C., Espinosa, J., Martínez, D., Olmedo, B., Espinoza, C. E. O., Núñez, R., Haylock, M., Benavides, H., and Mayorga, R.: Changes in precipitation and temperature extremes in Central America and northern South America, 1961–2003, Journal of Geophysical Research: Atmospheres, 110, https://doi.org/https://doi.org/10.1029/2005JD006119, 2005.

Alpert, P., Ben-Gai, T., Baharad, A., Benjamini, Y., Yekutieli, D., Colacino, M., Diodato, L., Ramis, C., Homar, V., Romero, R., Michaelides, S., and Manes, A.: The paradoxical increase of Mediterranean extreme daily rainfall in spite of decrease in total values, Geophysical Research Letters, 29, 31–1–31–4, https://doi.org/https://doi.org/10.1029/2001GL013554, 2002.

Amiri, A., Gumiere, S. J., Gharabaghi, B., and Bonakdari, H.: From warm seas to flooded streets: The impact of sea surface temperature on cutoff low and extreme rainfall in Valencia, Spain, Journal of Flood Risk Management, 18, e13 055, https://doi.org/10.1111/jfr3.13055, 2025.

Anav, A., Antonelli, M., Calmanti, S., Carillo, A., Catalano, F., Dell'Aquila, A., Iacono, R., Marullo, S., Napolitano, E., Palma, M., Pisacane, G., Sannino, G., and Struglia, M. V.: Dynamical downscaling of CMIP6 scenarios with ENEA-REG: an impact-oriented application for the Med-CORDEX region, Climate Dynamics, 62, 3261 – 3287, https://doi.org/10.1007/s00382-023-07064-3, 2024.

Armon, M., Marra, F., Enzel, Y., Rostkier-Edelstein, D., Garfinkel, C. I., Adam, O., Dayan, U., and Morin, E.: Reduced Rainfall in Future Heavy Precipitation Events Related to Contracted Rain Area Despite Increased Rain Rate, Earth's Future, 10, e2021EF002 397, https://doi.org/https://doi.org/10.1029/2021EF002397, e2021EF002397 2021EF002397, 2022.

Armon, M., Shmilovitz, Y., and Dente, E.: Anatomy of a foreseeable disaster: Lessons from the 2023 dam-breaching flood in Derna, Libya, Science Advances, 11, eadu2865, https://doi.org/10.1126/sciadv.adu2865, 2025.

Arrighi, C. and Domeneghetti, A.: Brief communication: On the environmental impacts of the 2023 floods in Emilia-Romagna (Italy), Natural Hazards and Earth System Sciences, 24, 673–679, https://doi.org/10.5194/nhess-24-673-2024, 2024.

Avino, A., Cimorelli, L., Furcolo, P., Noto, L. V., Pelosi, A., Pianese, D., Villani, P., and Manfreda, S.: Are rainfall extremes increasing in southern Italy?, Journal of Hydrology, 631, 130 684, https://doi.org/10.1016/j.jhydrol.2024.130684, 2024.

Avolio, E. and Federico, S.: WRF simulations for a heavy rainfall event in southern Italy: Verification and sensitivity tests, Atmospheric Research, 209, 14–35, https://doi.org/10.1016/j.atmosres.2018.03.009, 2018.

Avolio, E., Cavalcanti, O., Furnari, L., Senatore, A., and Mendicino, G.: Brief communication: Preliminary hydro-meteorological analysis of the flash flood of 20 August 2018 in Raganello Gorge, southern Italy, Natural Hazards and Earth System Sciences, 19, 1619–1627, https://doi.org/10.5194/nhess-19-1619-2019, 2019.

Babaousmail, H., Hou, R., Ayugi, B., Sian, K. T. C. L. K., Ojara, M., Mumo, R., Chehbouni, A., and Ongoma, V.: Future changes in mean and extreme precipitation over the Mediterranean and Sahara regions using bias-corrected CMIP6 models, International Journal of Climatology, 42, 7280–7297, https://doi.org/https://doi.org/10.1002/joc.7644, 2022.

Ban, N., Schmidli, J., and Schär, C.: Evaluation of the convection-resolving regional climate modeling approach in decade-long simulations, Journal of Geophysical Research: Atmospheres, 119, 7889–7907, https://doi.org/https://doi.org/10.1002/2014JD021478, 2014.

Bentsen, M., Oliviè, D. J. L., Seland, y., Toniazzo, T., Gjermundsen, A., Graff, L. S., Debernard, J. B., Gupta, A. K., He, Y., Kirkevåg, A., Schwinger, J., Tjiputra, J., Aas, K. S., Bethke, I., Fan, Y., Griesfeller, J., Grini, A., Guo, C., Ilicak, M., Karset, I. H. H., Landgren, O. A.,

Liakka, J., Moseid, K. O., Nummelin, A., Spensberger, C., Tang, H., Zhang, Z., Heinze, C., Iversen, T., and Schulz, M.: IPCC DDC: NCC NorESM2-MM model output prepared for CMIP6 CMIP, https://doi.org/10.26050/WDCC/AR6.C6CMNCCN2, 2023.

Beranová, R., Huth, R., and Vít, V.: A multi-dataset analysis of precipitation trends in Europe, Journal of Hydrometeorology, https://doi.org/10.1175/JHM-D-24-0114.1, 2025.

Berthou, S., Mailler, S., Drobinski, P., Arsouze, T., Bastin, S., Béranger, K., Flaounas, E., Lebeaupin Brossier, C., Somot, S., and Stéfanon, M.: Influence of submonthly air–sea coupling on heavy precipitation events in the Western Mediterranean basin, Quarterly Journal of the Royal Meteorological Society, 142, 453 – 471, https://doi.org/10.1002/qj.2717, 2016.

Blöschl, G., Hall, J., Viglione, A., et al.: Changing climate both increases and decreases European river floods, Nature, 573, 108–111, https://doi.org/10.1038/s41586-019-1495-6, 2019.

Boucher, O., Denvil, S., Levavasseur, G., Cozic, A., Caubel, A., Foujols, M.-A., Meurdesoif, Y., Cadule, P., Devilliers, M., Ghattas, J., Lebas, N., Lurton, T., Mellul, L., Musat, I., Mignot, J., and Cheruy, F.: IPCC DDC: IPSL IPSL-CM6A-LR model output prepared for CMIP6 CMIP, https://doi.org/10.26050/WDCC/AR6.C6CMIPICL, 2023.

Buttafuoco, G., Caloiero, T., and Coscarelli, R.: Spatial and temporal patterns of the mean annual precipitation at decadal time scale in southern Italy (Calabria region), Theoretical and Applied Climatology, 105, 431–444, https://doi.org/10.1007/s00704-011-0398-8, 2011.

Caloiero, T., Coscarelli, R., Ferrari, E., and Sirangelo, B.: Temporal analysis of rainfall categories in Southern Italy (Calabria Region), Environmental Processes, 4, 113–124, https://doi.org/10.1007/s40710-017-0215-1, 2017.

Caloiero, T., Filice, E., Coscarelli, R., and Pellicone, G.: A Homogeneous Dataset for Rainfall Trend Analysis in the Calabria Region (Southern Italy), Water, 12, 2541, https://doi.org/10.3390/w12092541, 2020.

Caloiero, T., Coscarelli, R., and Pellicone, G.: Trend Analysis of Rainfall Using Gridded Data over a Region of Southern Italy, Water, 13, 2271, https://doi.org/10.3390/w13162271, 2021.

Cammalleri, C., Spinoni, J., Barbosa, P., Toreti, A., and Vogt, J. V.: The effects of non-stationarity on SPI for operational drought monitoring in Europe, International Journal of Climatology, 42, 3418–3430, https://doi.org/10.1002/joc.7424, 2022.

Cammalleri, C., Sarwar, A. N., Avino, A., Nikravesh, G., Bonaccorso, B., Mendicino, G., Senatore, A., and Manfreda, S.: Testing trends in gridded rainfall datasets at relevant hydrological scales: A comparative study with regional ground observations in Southern Italy, Journal of Hydrology: Regional Studies, 55, 101 950, https://doi.org/10.1016/j.ejrh.2024.101950, 2024.

Chadwick, R.: Sub-tropical drying explained, Nature Clim Change, 7, 10–11, https://doi.org/10.1038/nclimate3167, 2017.

Cheng, L., Abraham, J., Trenberth, K. E., Boyer, T., Mann, M. E., Zhu, J., Wang, F., and Yu, F.: New Record Ocean Temperatures and Related Climate Indicators in 2023, Advances in Atmospheric Sciences, https://doi.org/10.1007/s00376-024-3378-5, 2024.

Cheng, L., Abraham, J., Trenberth, K. E., Reagan, J., Zhang, H.-M., Storto, A., Von Schuckmann, K., Pan, Y., Zhu, Y., Mann, M. E., et al.: Record High Temperatures in the Ocean in 2024, Advances in Atmospheric Sciences, pp. 1–18, https://doi.org/10.1007/s00376-025-4541-3, 2025.

(CMEMS), E. C. M. S. I.: ESA SST CCI and C3S reprocessed sea surface temperature analyses, https://doi.org/doi.org/10.48670/moi-00169, accessed on 09-Oct-2024, 2023.

Colacino, M., Conte, M., and Piervitali, E.: Elementi di climatologia della Calabria, IFA-CNR, Rome, 1997.

Coppola, E., Sobolowski, S., Pichelli, E., Raffaele, F., Ahrens, B., Anders, I., Ban, N., Bastin, S., Belda, M., Belusic, D., et al.: A first-of-its-kind multi-model convection permitting ensemble for investigating convective phenomena over Europe and the Mediterranean, Climate Dynamics, 55, 3–34, 2020.

Cornes, R. C., van der Schrier, G., van den Besselaar, E. J. M., and Jones, P. D.: An Ensemble Version of the E-OBS Temperature and Precipitation Data Sets, Journal of Geophysical Research: Atmospheres, 123, 9391–9409, https://doi.org/https://doi.org/10.1029/2017JD028200, 2018.

Danabasoglu, G.: IPCC DDC: NCAR CESM2-WACCM model output prepared for CMIP6 CMIP, https://doi.org/10.26050/WDCC/AR6.C6CMNRCESWA, 2023.

Dix, M., Bi, D., Dobrohotoff, P., Fiedler, R., Harman, I., Law, R., Mackallah, C., Marsland, S., O'Farrell, S., Rashid, H., Srbinovsky, J., Sullivan, A., Trenham, C., Vohralik, P., Watterson, I., Williams, G., Woodhouse, M., Bodman, R., Dias, F. B., Domingues, C. M., Hannah, N., Heerdegen, A., Savita, A., Wales, S., Allen, C., Druken, K., Evans, B., Richards, C., Ridzwan, S. M., Roberts, D., Smillie, J., Snow, K., Ward, M., and Yang, R.: IPCC DDC: CSIRO-ARCCSS ACCESS-CM2 model output prepared for CMIP6 CMIP, https://doi.org/10.26050/WDCC/AR6.C6CMCSIACC, 2023.

Donat, M. G., Alexander, L. V., Yang, H., Durre, I., Vose, R., Dunn, R. J. H., Willett, K. M., Aguilar, E., Brunet, M., Caesar, J., Hewitson, B., Jack, C., Klein Tank, A. M. G., Kruger, A. C., Marengo, J., Peterson, T. C., Renom, M., Oria Rojas, C., Rusticucci, M., Salinger, J., Elrayah, A. S., Sekele, S. S., Srivastava, A. K., Trewin, B., Villarroel, C., Vincent, L. A., Zhai, P., Zhang, X., and Kitching, S.: Updated analyses of temperature and precipitation extreme indices since the beginning of the twentieth century: The HadEX2 dataset, Journal of Geophysical Research: Atmospheres, 118, 2098–2118, https://doi.org/https://doi.org/10.1002/jgrd.50150, 2013.

Dutheil, C., Bador, M., Lengaigne, M., Lefèvre, J., Jourdain, N., Vialard, J., Jullien, S., Peltier, A., and Menkes, C.: Impact of surface temperature biases on climate change projections of the South Pacific Convergence Zone, Climate Dynamics, 53, 1–23, https://doi.org/10.1007/s00382-019-04692-6, 2019.

(EC-Earth), E.-E. C.: IPCC DDC: EC-Earth-Consortium EC-Earth-3-CC model output prepared for CMIP6 CMIP, https://doi.org/10.26050/WDCC/AR6.C6CMEEEEC, 2023.

Federico, S., Avolio, E., Pasqualoni, L., De Leo, L., Sempreviva, A. M., and Bellecci, C.: Preliminary results of a 30-year daily rainfall data base in southern Italy, Atmospheric Research, 94, 641–651, https://doi.org/10.1016/j.atmosres.2009.03.008, 2009.

Fernández-Alvarez, J. C., Pérez-Alarcón, A., Eiras-Barca, J., Rahimi, S., Nieto, R., and Gimeno, L.: Projected changes in atmospheric moisture transport contributions associated with climate warming in the North Atlantic, Nature Communications, 14, https://doi.org/10.1038/s41467-023-41915-1, 2023.

Ferrari, A., Passadore, G., Vacondio, R., Carniello, L., Pivato, M., Crestani, E., Carraro, F., Aureli, F., Carta, S., Stumpo, F., and Mignosa, P.: Brief communication: Hydrological and hydraulic investigation of the extreme September 2024 flood on the Lamone River in Emilia-Romagna, Italy, Natural Hazards and Earth System Sciences, 25, https://doi.org/10.5194/nhess-25-2473-2025, 2025.

Field, P. R. and Wood, R.: Precipitation and Cloud Structure in Midlatitude Cyclones, Journal of Climate, 20, 233 – 254, https://doi.org/10.1175/JCLI3998.1, 2007.

Fita, L., Romero, R., De Luque Söllheim, A., Emanuel, K., and Ramis, C.: Analysis of the environments of seven Mediterranean tropical-like storms using an axisymmetric, nonhydrostatic, cloud resolving model, Nat. Hazards Earth Syst. Sci, 7, https://doi.org/10.5194/nhess-7-41-2007, 2007.

Flaounas, E., Davolio, S., Raveh-Rubin, S., Pantillon, F., Miglietta, M. M., Gaertner, M. A., Hatzaki, M., Homar, V., Khodayar, S., Korres, G., Kotroni, V., Kushta, J., Reale, M., and Ricard, D.: Mediterranean cyclones: current knowledge and open questions on dynamics, prediction, climatology and impacts, Weather and Climate Dynamics, 3, 173–208, https://doi.org/10.5194/wcd-3-173-2022, 2022.

Flaounas, E., Dafis, S., Davolio, S., Faranda, D., Ferrarin, C., Hartmuth, K., Hochman, A., Koutroulis, A., Khodayar, S., Miglietta, M. M., Pantillon, F., Patlakas, P., Sprenger, M., and Thurnherr, I.: Dynamics, predictability, impacts, and climate change considerations of the catastrophic Mediterranean Storm Daniel (2023), EGUsphere, 2024, 1–29, https://doi.org/10.5194/egusphere-2024-2809, 2024.

Fosser, G., Gaetani, M., Kendon, E. J., Adinolfi, M., Ban, N., Belušić, D., Caillaud, C., Careto, J. A., Coppola, E., Demory, M.-E., et al.: Convection-permitting climate models offer more certain extreme rainfall projections, NPJ Climate and atmospheric science, 7, 51, 2024.

Furnari, L., Magnusson, L., Mendicino, G., and Senatore, A.: Fully coupled high-resolution medium-range forecasts: Evaluation of the hydrometeorological impact in an ensemble framework, Hydrological Processes, 36, e14 503, https://doi.org/10.1002/hyp.14503, 2022.

Fusto, F., Marsico, L., and Rotundo, R.: Evento Meteopluviometrico del 23-25 novembre 2019. Rapporto di Evento, https://www.cfd.calabria.it//DatiVari/Pubblicazioni/rapporto%20evento%2023-25%20novembre%202019.pdf, in italian, last access 17 Feb 2025, 2019.

Giorgi, F.: Climate change hot-spots, Geophysical Research Letters, 33, https://doi.org/https://doi.org/10.1029/2006GL025734, 2006.

Gomis-Cebolla, J., Rattayova, V., Salazar-Galán, S., and Francés, F.: Evaluation of ERA5 and ERA5-Land reanalysis precipitation datasets over Spain (1951–2020), Atmospheric Research, 284, 106 606, https://doi.org/10.1016/j.atmosres.2023.106606, 2023.

González-Rouco, J. F., Jiménez, J. L., Quesada, V., and Valero, F.: Quality control and homogeneity of precipitation data in the southwest of Europe, Journal of climate, 14, 964–978, 2001.

Guo, C., Ning, N., Guo, H., Tian, Y., Bao, A., and De Maeyer, P.: Does ERA5-Land Effectively Capture Extreme Precipitation in the Yellow River Basin?, Atmosphere, 15, 1254, https://doi.org/10.3390/atmos15101254, 2024.

Hamed, K. H. and Rao, A. R.: A modified Mann-Kendall trend test for autocorrelated data, Journal of hydrology, 204, 182–196, https://doi.org/10.1016/S0022-1694(97)00125-X, 1998.

Hausfather, Z. and Peters, G. P.: Emissions – the 'business as usual' story is misleading, Nature, 577, 618 – 620, https://doi.org/10.1038/d41586-020-00177-3, 2020.

He, J. and Soden, B. J.: A re-examination of the projected subtropical precipitation decline, Nature Climate Change, 7, 53 – 57, https://doi.org/10.1038/nclimate3157, 2017.

Hersbach, H., Bell, B., Berrisford, P., Hirahara, S., Horányi, A., Muñoz-Sabater, J., Nicolas, J., Peubey, C., Radu, R., Schepers, D., et al.: The ERA5 global reanalysis, Quarterly Journal of the Royal Meteorological Society, 146, 1999–2049, https://doi.org/10.1002/qj.3803, 2020.

Hochman, A., Harpaz, T., Saaroni, H., and Alpert, P.: The seasons' length in 21st century CMIP5 projections over the eastern Mediterranean, International Journal of Climatology, 38, 2627–2637, https://doi.org/https://doi.org/10.1002/joc.5448, 2018.

Hong, S.-Y., Noh, Y., and Dudhia, J.: A New Vertical Diffusion Package with an Explicit Treatment of Entrainment Processes, Monthly Weather Review, 134, 2318 – 2341, https://doi.org/10.1175/MWR3199.1, 2006.

Hosseinzadehtalaei, P., Tabari, H., and Willems, P.: Climate change impact on short-duration extreme precipitation and intensity–duration–frequency curves over Europe, Journal of Hydrology, 590, 125 249, https://doi.org/10.1016/j.jhydrol.2020.125249, 2020.

Instituto de Física de Cantabria (IFCA), C.: IPCC-WGI AR6 Interactive Atlas Dataset: CMIP6, https://doi.org/10.20350/digitalCSIC/15492, 2023.

Ippolito, M., De Caro, D., Cannarozzo, M., Provenzano, G., and Ciraolo, G.: Evaluation of daily crop reference evapotranspiration and sensitivity analysis of FAO Penman-Monteith equation using ERA5-Land reanalysis database in Sicily, Italy, Agricultural Water Management, 295, 108 732, https://doi.org/10.1016/j.agwat.2024.108732, 2024.

Jacob, D., Petersen, J., Eggert, B., Alias, A., Christensen, O. B., Bouwer, L. M., Braun, A., Colette, A., Déqué, M., Georgievski, G., et al.: EURO-CORDEX: new high-resolution climate change projections for European impact research, Regional environmental change, 14, 563–578, https://doi.org/10.1007/s10113-013-0499-2, 2014.

Janjić, Z. I.: The Step-Mountain Eta Coordinate Model: Further Developments of the Convection, Viscous Sublayer, and Turbulence Closure Schemes, Monthly weather review, 122, 927–945, https://doi.org/10.1175/1520-0493(1994)122<0927:TSMECM>2.0.CO;2, 1994.

Jungclaus, J., Bittner, M., Wieners, K.-H., Wachsmann, F., Schupfner, M., Legutke, S., Giorgetta, M., Reick, C., Gayler, V., Haak, H., de Vrese, P., Raddatz, T., Esch, M., Mauritsen, T., von Storch, J.-S., Behrens, J., Brovkin, V., Claussen, M., Crueger, T., Fast, I., Fiedler, S., Hagemann, S., Hohenegger, C., Jahns, T., Kloster, S., Kinne, S., Lasslop, G., Kornblueh, L., Marotzke, J., Matei, D., Meraner, K., Mikolajewicz, U., Modali, K., Müller, W., Nabel, J., Notz, D., Peters-von Gehlen, K., Pincus, R., Pohlmann, H., Pongratz, J., Rast, S., Schmidt, H., Schnur, R., Schulzweida, U., Six, K., Stevens, B., Voigt, A., and Roeckner, E.: IPCC DDC: MPI-M MPIESM1.2-HR model output prepared for CMIP6 CMIP, https://doi.org/10.26050/WDCC/AR6.C6CMMXME2, 2023.

Kendall, M.: Rank Correlation Methods, C. Griffin, https://books.google.it/books?id=hiBMAAAAMAAJ, 1948.

Khodayar, S., Davolio, S., Di Girolamo, P., Lebeaupin Brossier, C., Flaounas, E., Fourrie, N., Lee, K.-O., Ricard, D., Vie, B., Bouttier, F., et al.: Overview towards improved understanding of the mechanisms leading to heavy precipitation in the western Mediterranean: lessons learned from HyMeX, Atmospheric Chemistry and Physics, 21, 17 051–17 078, https://doi.org/10.5194/acp-21-17051-2021, 2021.

Kömüşcü, A. Ü. and Oğuz, K.: Analysis of cold anomalies observed over Turkey during the 2018/2019 winter in relation to polar vortex and other atmospheric patterns, Meteorology and Atmospheric Physics, 133, 1327–1354, https://doi.org/10.1007/s00703-021-00806-0, 2021.

Krasting, J. P., John, J. G., Blanton, C., McHugh, C., Nikonov, S., Radhakrishnan, A., Rand, K., Zadeh, N. T., Balaji, V., Durachta, J., Dupuis, C., Menzel, R., Robinson, T., Underwood, S., Vahlenkamp, H., Dunne, K. A., Gauthier, P. P., Ginoux, P., Griffies, S. M., Hallberg, R., Harrison, M., Hurlin, W., Malyshev, S., Naik, V., Paulot, F., Paynter, D. J., Ploshay, J., Reichl, B. G., Schwarzkopf, D. M., Seman, C. J., Silvers, L., Wyman, B., Zeng, Y., Adcroft, A., Dunne, J. P., Dussin, R., Guo, H., He, J., Held, I. M., Horowitz, L. W., Lin, P., Milly, P., Shevliakova, E., Stock, C., Winton, M., Wittenberg, A. T., Xie, Y., and Zhao, M.: IPCC DDC: NOAA-GFDL GFDL-ESM4 model output prepared for CMIP6 CMIP, https://doi.org/10.26050/WDCC/AR6.C6CMNGGFE, 2023.

Lazoglou, G., Papadopoulos-Zachos, A., Georgiades, P., Zittis, G., Velikou, K., Manios, E. M., and Anagnostopoulou, C.: Identification of climate change hotspots in the Mediterranean, Scientific Reports, 14, 29 817, https://doi.org/10.1038/s41598-024-80139-1, 2024.

Lee, E. and Hong, S.-Y.: Impact of the Sea Surface Salinity on Simulated Precipitation in a Global Numerical Weather Prediction Model, Journal of Geophysical Research: Atmospheres, 124, 719–730, https://doi.org/https://doi.org/10.1029/2018JD029591, 2019.

Li, L.: IPCC DDC: CAS FGOALS-g3 model output prepared for CMIP6 ScenarioMIP, https://doi.org/10.26050/WDCC/AR6.C6SPCASFGO, 2023.

Lin, K.-J., Yang, S.-C., and Chen, S. S.: Sensitivity of Extreme Rainfall in Taiwan to SST Over the South China Sea Through Modulation of Marine Boundary Layer Jet: A Mei-Yu Front Event During 1–4 June 2017, Geophysical Research Letters, 50, e2023GL104 441, https://doi.org/https://doi.org/10.1029/2023GL104441, e2023GL104441 2023GL104441, 2023.

Lionello, P. and Scarascia, L.: The relation between climate change in the Mediterranean region and global warming, Regional Environmental Change, 18, 1481–1493, https://doi.org/10.1007/s10113-018-1290-1, 2018.

Llasat, M., Llasat-Botija, M., Petrucci, O., Pasqua, A., Rosselló, J., Vinet, F., and Boissier, L.: Towards a database on societal impact of Mediterranean floods within the framework of the HYMEX project, Natural Hazards and Earth System Sciences, 13, 1337–1350, https://doi.org/10.5194/nhess-13-1337-2013, 2013.

Lovato, T. and Peano, D.: IPCC DDC: CMCC CMCC-CM2-SR5 model output prepared for CMIP6 CMIP, https://doi.org/10.26050/WDCC/AR6.C6CMCMCCS, 2023.

Mann, H. B.: Nonparametric tests against trend, Econometrica: Journal of the econometric society, pp. 245–259, https://doi.org/10.2307/1907187, 1945.

Marsico, L. and Rotundo, R.: Evento Meteopluviometrico del 11-13 novembre 2019. Rapporto di Evento, https://www.cfd.calabria.it//DatiVari/Pubblicazioni/rapporto%20evento%2011-13%20novembre%202019.pdf, in italian, last access 17 Feb 2025, 2019.

Masson-Delmotte, V., Zhai, P., Pirani, A., Connors, S. L., Péan, C., Berger, S., Caud, N., Chen, Y., Goldfarb, L., Gomis, M., et al.: Climate Change 2021: the Physical Science Basis, Contribution of working group I to the sixth assessment report of the intergovernmental panel on climate change, 2, 2391, https://doi.org/10.1017/9781009157896, 2021.

Mastrantonas, N., Furnari, L., Magnusson, L., Senatore, A., Mendicino, G., Pappenberger, F., and Matschullat, J.: Forecasting extreme precipitation in the central Mediterranean: Changes in predictors' strength with prediction lead time, Meteorological Applications, 29, e2101, https://doi.org/https://doi.org/10.1002/met.2101, 2022.

Matsui, T., Zhang, S. Q., Lang, S. E., Tao, W.-K., Ichoku, C., and Peters-Lidard, C. D.: Impact of radiation frequency, precipitation radiative forcing, and radiation column aggregation on convection-permitting West African monsoon simulations, Climate Dynamics, 55, 193–213, https://doi.org/10.1007/s00382-018-4187-2, 2020.

Matte, D., Christensen, J. H., and Ozturk, T.: Spatial extent of precipitation events: when big is getting bigger, Climate Dynamics, 58, 1861–1875, https://doi.org/10.1007/s00382-021-05998-0, 2022.

Meehl, G. A., Karl, T., Easterling, D. R., Changnon, S., Pielke, R., Changnon, D., Evans, J., Groisman, P. Y., Knutson, T. R., Kunkel, K. E., Mearns, L. O., Parmesan, C., Pulwarty, R., Root, T., Sylves, R. T., Whetton, P., and Zwiers, F.: An Introduction to Trends in Extreme Weather and Climate Events: Observations, Socioeconomic Impacts, Terrestrial Ecological Impacts, and Model Projections, Bulletin of the American Meteorological Society, 81, 413 – 416, https://doi.org/10.1175/1520-0477(2000)081<0413:AITTIE>2.3.CO;2, 2000.

Meinshausen, M., Nicholls, Z. R. J., Lewis, J., Gidden, M. J., Vogel, E., Freund, M., Beyerle, U., Gessner, C., Nauels, A., Bauer, N., Canadell, J. G., Daniel, J. S., John, A., Krummel, P. B., Luderer, G., Meinshausen, N., Montzka, S. A., Rayner, P. J., Reimann, S., Smith, S. J., van den Berg, M., Velders, G. J. M., Vollmer, M. K., and Wang, R. H. J.: The shared socio-economic pathway (SSP) greenhouse gas concentrations and their extensions to 2500, Geoscientific Model Development, 13, 3571–3605, https://doi.org/10.5194/gmd-13-3571-2020, 2020.

Mendicino, G. and Versace, P.: Integrated drought watch system: a case study in Southern Italy, Water resources management, 21, 1409–1428, https://doi.org/10.1007/s11269-006-9091-6, 2007.

Menemenlis, S., Vecchi, G., Yang, W., Fueglistaler, S., and Raghuraman, S. P.: Consequential differences in satellite-era sea surface temperature trends across datasets, Nature Climate Change, 15, 897–903, https://doi.org/10.1038/s41558-025-02362-6, 2025.

Meredith, E. P., Semenov, V. A., Maraun, D., Park, W., and Chernokulsky, A. V.: Crucial role of Black Sea warming in amplifying the 2012 Krymsk precipitation extreme, Nature Geoscience, 8, 615–619, https://doi.org/10.1038/ngeo2483, 2015.

Miglietta, M. M. and Rotunno, R.: Development mechanisms for Mediterranean tropical-like cyclones (medicanes), Quarterly Journal of the Royal Meteorological Society, 145, 1444–1460, https://doi.org/10.1002/qj.3503, 2019.

Miglietta, M. M., Moscatello, A., Conte, D., Mannarini, G., Lacorata, G., and Rotunno, R.: Numerical analysis of a Mediterranean 'hurricane'over south-eastern Italy: Sensitivity experiments to sea surface temperature, Atmospheric research, 101, 412–426, https://doi.org/10.1016/j.atmosres.2011.04.006, 2011.

Miglietta, M. M., Flaounas, E., González-Alemán, J. J., Panegrossi, G., Gaertner, M. A., Pantillon, F., Pasquero, C., Schultz, D. M., D'Adderio, L. P., Dafis, S., Husson, R., Ricchi, A., Carrió, D. S. C., Davolio, S., Fita, L., Picornell, M. A., Pytharoulis, I., Raveh-Rubin, S., Scoccimarro, E., Bernini, L., Cavicchia, L., Conte, D., Ferretti, R., Flocas, H., Gutiérrez-Fernández, J., Hatzaki, M., Santaner, V. H., Jansà, A., and Patlakas, P.: Defining Medicanes: Bridging the Knowledge Gap Between Tropical and Extratropical Cyclones in the Mediterranean, Bulletin of the American Meteorological Society, pp. BAMS–D–24–0289.1, https://doi.org/10.1175/BAMS-D-24-0289.1, 2025.

Mlawer, E. J., Taubman, S. J., Brown, P. D., Iacono, M. J., and Clough, S. A.: Radiative transfer for inhomogeneous atmospheres: RRTM, a validated correlated-k model for the longwave, Journal of Geophysical Research: Atmospheres, 102, 16 663–16 682, https://doi.org/10.1029/97JD00237, 1997.

Mohamed, B., Abdallah, A. M., Alam El-Din, K., Nagy, H., and Shaltout, M.: Inter-Annual Variability and Trends of Sea Level and Sea Surface Temperature in the Mediterranean Sea over the Last 25 years, Pure and Applied Geophysics, 176, 3787–3810, https://doi.org/10.1007/s00024-019-02156-w, 2019.

Muñoz-Sabater, J., Dutra, E., Agustí-Panareda, A., Albergel, C., Arduini, G., Balsamo, G., Boussetta, S., Choulga, M., Harrigan, S., Hersbach, H., et al.: ERA5-Land: A state-of-the-art global reanalysis dataset for land applications, Earth system science data, 13, 4349–4383, https://doi.org/10.5194/essd-13-4349-2021, 2021.

Müller, S. K., Pichelli, E., Coppola, E., Berthou, S., Brienen, S., Caillaud, C., Demory, M.-E., Dobler, A., Feldmann, H., Mercogliano, P., Tölle, M., and de Vries, H.: The climate change response of alpine-mediterranean heavy precipitation events, Climate Dynamics, 62, 165 – 186, https://doi.org/10.1007/s00382-023-06901-9, 2024.

Necker, T., Wolfgruber, L., Kugler, L., Weissmann, M., Dorninger, M., and Serafin, S.: The fractions skill score for ensemble forecast verification, Quarterly Journal of the Royal Meteorological Society, 150, 4457–4477, https://doi.org/10.1002/qj.4824, 2024.

Niu, G.-Y., Yang, Z.-L., Mitchell, K. E., Chen, F., Ek, M. B., Barlage, M., Kumar, A., Manning, K., Niyogi, D., Rosero, E., et al.: The community Noah land surface model with multiparameterization options (Noah-MP): 1. Model description and evaluation with local-scale measurements, Journal of Geophysical Research: Atmospheres, 116, https://doi.org/10.1029/2010JD015139, 2011.

Noyelle, R., Ulbrich, U., Becker, N., and Meredith, E. P.: Assessing the impact of sea surface temperatures on a simulated medicane using ensemble simulations, Natural Hazards and Earth System Sciences, 19, 941–955, https://doi.org/10.5194/nhess-19-941-2019, 2019.

Panickal, S., Raghavan, K., Gopinathan, P. A., Narayanasetti, S., Choudhury, A. D., Singh, M., and Modi, A.: IPCC DDC: CCCR-IITM IITM-ESM model output data prepared for CMIP6 CMIP/DECK, https://doi.org/10.26050/WDCC/AR6.C6CMCIIIT, 2023.

Pastor, F., Valiente, J. A., and Khodayar, S.: A Warming Mediterranean: 38 Years of Increasing Sea Surface Temperature, Remote sensing, 12, 2687, https://doi.org/https://doi.org/10.3390/rs12172687, 2020.

Petrucci, O., Salvati, P., Aceto, L., Bianchi, C., Pasqua, A. A., Rossi, M., and Guzzetti, F.: The Vulnerability of People to Damaging Hydrogeological Events in the Calabria Region (Southern Italy), International Journal of Environmental Research and Public Health, 15, 48, https://doi.org/10.3390/ijerph15010048, 2018.

Pfahl, S., O'Gorman, P., and Fischer, E.: Understanding the regional pattern of projected future changes in extreme precipitation, Nature Climate Change, 7, 423 – 427, https://doi.org/10.1038/nclimate3287, 2017.

Pichelli, E., Coppola, E., Sobolowski, S., Ban, N., Giorgi, F., Stocchi, P., Alias, A., Belušić, D., Berthou, S., Caillaud, C., et al.: The first multi-model ensemble of regional climate simulations at kilometer-scale resolution part 2: historical and future simulations of precipitation, Climate Dynamics, 56, 3581–3602, 2021.

Pilatin, H., Yucel, I., Duzenli, E., and Yilmaz, M. T.: Sensitivity of WRF-derived hydrometeorological extremes to sea surface temperatures in regions with complex topography and diverse climate, Atmospheric Research, 264, 105 816, 2021.

Prein, A. F., Langhans, W., Fosser, G., Ferrone, A., Ban, N., Goergen, K., Keller, M., Tölle, M., Gutjahr, O., Feser, F., Brisson, E., Kollet, S., Schmidli, J., van Lipzig, N. P. M., and Leung, R.: A review on regional convection-permitting climate modeling: Demonstrations, prospects, and challenges, Reviews of Geophysics, 53, 323–361, https://doi.org/https://doi.org/10.1002/2014RG000475, 2015.

Prete, G., Avolio, E., Capparelli, V., Lepreti, F., and Carbone, V.: Daily Precipitation and Temperature Extremes in Southern Italy (Calabria Region), Atmosphere, 14, 553, https://doi.org/10.3390/atmos14030553, 2023.

Pytharoulis, I.: Analysis of a Mediterranean tropical-like cyclone and its sensitivity to the sea surface temperatures, Atmospheric Research, 208, 167–179, https://doi.org/10.1016/j.atmosres.2017.08.009, 2018.

Rasmussen, R., Liu, C., Ikeda, K., Gochis, D., Yates, D., Chen, F., Tewari, M., Barlage, M., Dudhia, J., Yu, W., Miller, K., Arsenault, K., Grubišić, V., Thompson, G., and Gutmann, E.: High-Resolution Coupled Climate Runoff Simulations of Seasonal Snowfall over Colorado: A Process Study of Current and Warmer Climate, Journal of Climate, 24, 3015 – 3048, https://doi.org/10.1175/2010JCLI3985.1, 2011.

Reale, M., Cabos Narvaez, W. D., Cavicchia, L., Conte, D., Coppola, E., Flaounas, E., Giorgi, F., Gualdi, S., Hochman, A., Li, L., et al.: Future projections of Mediterranean cyclone characteristics using the Med-CORDEX ensemble of coupled regional climate system models, Climate dynamics, pp. 1–24, https://doi.org/10.1007/s00382-021-06018-x, 2022.

Ricchi, A., Miglietta, M. M., Barbariol, F., Benetazzo, A., Bergamasco, A., Bonaldo, D., Cassardo, C., Falcieri, F. M., Modugno, G., Russo, A., et al.: Sensitivity of a Mediterranean tropical-like cyclone to different model configurations and coupling strategies, Atmosphere, 8, 92, https://doi.org/10.3390/atmos8050092, 2017.

Ricchi, A., Sangelantoni, L., Redaelli, G., Mazzarella, V., Montopoli, M., Miglietta, M. M., Tiesi, A., Mazzà, S., Rotunno, R., and Ferretti, R.: Impact of the SST and topography on the development of a large-hail storm event, on the Adriatic Sea, Atmospheric Research, 296, 107 078, https://doi.org/10.1016/j.atmosres.2023.107078, 2023.

Roberts, N. M. and Lean, H. W.: Scale-Selective Verification of Rainfall Accumulations from High-Resolution Forecasts of Convective Events, Monthly Weather Review, 136, 78 – 97, https://doi.org/10.1175/2007MWR2123.1, 2008.

Rong, X.: IPCC DDC: CAMS CAMS_CSM1.0 model output prepared for CMIP6 CMIP, https://doi.org/10.26050/WDCC/AR6.C6CMCAMCC0, 2023.

Sannino, G., Carillo, A., Iacono, R., Napolitano, E., Palma, M., Pisacane, G., and Struglia, M.: Modelling present and future climate in the Mediterranean Sea: a focus on sea-level change, Climate Dynamics, 59, 357–391, https://doi.org/10.1007/s00382-021-06132-w, 2022.

Schwalm, C. R., Glendon, S., and Duffy, P. B.: RCP8.5 tracks cumulative CO2 emissions, Proceedings of the National Academy of Sciences of the United States of America, 117, 19 656 – 19 657, https://doi.org/10.1073/PNAS.2007117117, 2020.

Seferian, R.: IPCC DDC: CNRM-CERFACS CNRM-ESM2-1 model output prepared for CMIP6 CMIP, https://doi.org/10.26050/WDCC/AR6.C6CMCECE1, 2023.

Seland, y., Bentsen, M., Oliviè, D. J. L., Toniazzo, T., Gjermundsen, A., Graff, L. S., Debernard, J. B., Gupta, A. K., He, Y., Kirkevåg, A., Schwinger, J., Tjiputra, J., Aas, K. S., Bethke, I., Fan, Y., Griesfeller, J., Grini, A., Guo, C., Ilicak, M., Karset, I. H. H., Landgren, O. A., Liakka, J., Moseid, K. O., Nummelin, A., Spensberger, C., Tang, H., Zhang, Z., Heinze, C., Iversen, T., and Schulz, M.: IPCC DDC: NCC NorESM2-LM model output prepared for CMIP6 CMIP, https://doi.org/10.26050/WDCC/AR6.C6CMNCCNL, 2023.

Semmler, T., Danilov, S., Rackow, T., Sidorenko, D., Barbi, D., Hegewald, J., Sein, D., Wang, Q., and Jung, T.: IPCC DDC: AWI AWI-CM1.1MR model output prepared for CMIP6 CMIP, https://doi.org/10.26050/WDCC/AR6.C6CMAWAWM, 2023.

Sen, P. K.: Estimates of the Regression Coefficient Based on Kendall's tau, Journal of the American statistical association, 63, 1379–1389, https://doi.org/10.1080/01621459.1968.10480934, 1968.

Senatore, A., Mendicino, G., Knoche, H. R., and Kunstmann, H.: Sensitivity of Modeled Precipitation to Sea Surface Temperature in Regions with Complex Topography and Coastlines: A Case Study for the Mediterranean, Journal of Hydrometeorology, 15, 2370–2396, https://doi.org/https://doi.org/10.1175/JHM-D-13-089.1, 2014.

Senatore, A., Davolio, S., Furnari, L., and Mendicino, G.: Reconstructing Flood Events in Mediterranean Coastal Areas Using Different Reanalyses and High-Resolution Meteorological Models, Journal of Hydrometeorology, 21, 1865–1887, https://doi.org/10.1175/JHM-D-19-0270.1, 2020a.

Senatore, A., Furnari, L., and Mendicino, G.: Impact of high-resolution sea surface temperature representation on the forecast of small Mediterranean catchments' hydrological responses to heavy precipitation, Hydrology and Earth System Sciences, 24, 269–291, https://doi.org/10.5194/hess-24-269-2020, 2020b.

Skamarock, W. C., Klemp, J. B., Dudhia, J., Gill, D. O., Liu, Z., Berner, J., Wang, W., Powers, J. G., Duda, M. G., Barker, D. M., and Huang, X. y.: A Description of the Advanced Research WRF Model Version 4, Tech. rep., NCAR, https://doi.org/10.5065/1dfh-6p97, 2021.

Soares, P. M., Careto, J. A., Cardoso, R. M., Goergen, K., Katragkou, E., Sobolowski, S., Coppola, E., Ban, N., Belušić, D., Berthou, S., et al.: The added value of km-scale simulations to describe temperature over complex orography: the CORDEX FPS-Convection multi-model ensemble runs over the Alps, Climate Dynamics, 62, 4491–4514, 2024.

Stahl, K., Tallaksen, L. M., Hannaford, J., and Van Lanen, H.: Filling the white space on maps of European runoff trends: estimates from a multi-model ensemble, Hydrology and Earth System Sciences, 16, 2035–2047, https://doi.org/10.5194/hess-16-2035-2012, 2012.

Stephenson, T. S., Vincent, L. A., Allen, T., Van Meerbeeck, C. J., McLean, N., Peterson, T. C., Taylor, M. A., Aaron-Morrison, A. P., Auguste, T., Bernard, D., Boekhoudt, J. R. I., Blenman, R. C., Braithwaite, G. C., Brown, G., Butler, M., Cumberbatch, C. J. M., Etienne-Leblanc, S., Lake, D. E., Martin, D. E., McDonald, J. L., Ozoria Zaruela, M., Porter, A. O., Santana Ramirez, M., Tamar, G. A., Roberts, B. A., Sallons Mitro, S., Shaw, A., Spence, J. M., Winter, A., and Trotman, A. R.: Changes in extreme temperature and precipitation in the Caribbean region, 1961–2010, International Journal of Climatology, 34, 2957–2971, https://doi.org/https://doi.org/10.1002/joc.3889, 2014.

Stocchi, P. and Davolio, S.: Intense air-sea exchanges and heavy orographic precipitation over Italy: The role of Adriatic sea surface temperature uncertainty, Atmospheric Research, 196, 62–82, https://doi.org/https://doi.org/10.1016/j.atmosres.2017.06.004, 2017.

Stone, D. A.: Winter isn't what it used to be, Nature Geoscience, 14, 712–713, https://doi.org/10.1038/s41561-021-00832-y, 2021.

Sun, X. and Wu, R.: Spatial scale dependence of the relationship between turbulent surface heat flux and SST, Climate Dynamics, 58, 1127–1145, https://doi.org/10.1007/s00382-021-05957-9, 2022.

Swart, N. C., Cole, J. N., Kharin, V. V., Lazare, M., Scinocca, J. F., Gillett, N. P., Anstey, J., Arora, V., Christian, J. R., Jiao, Y., Lee, W. G., Majaess, F., Saenko, O. A., Seiler, C., Seinen, C., Shao, A., Solheim, L., von Salzen, K., Yang, D., Winter, B., and Sigmond, M.: IPCC DDC: CCCma CanESM5 model output prepared for CMIP6 CMIP, https://doi.org/10.26050/WDCC/AR6.C6CMCCCE, 2023.

Tang, Y., Rumbold, S., Ellis, R., Kelley, D., Mulcahy, J., Sellar, A., Walton, J., and Jones, C.: IPCC DDC: MOHC UKESM1.0-LL model output prepared for CMIP6 CMIP, https://doi.org/10.26050/WDCC/AR6.C6CMMOU0, 2023.

Thompson, G., Field, P. R., Rasmussen, R. M., and Hall, W. D.: Explicit Forecasts of Winter Precipitation Using an Improved Bulk Microphysics Scheme. Part II: Implementation of a New Snow Parameterization, Monthly Weather Review, 136, 5095–5115, https://doi.org/10.1175/2008MWR2387.1, 2008.

Tiedtke, M.: A Comprehensive Mass Flux Scheme for Cumulus Parameterization in Large-Scale Models, Monthly weather review, 117, 1779–1800, https://doi.org/10.1175/1520-0493(1989)117<1779:ACMFSF>2.0.CO;2, 1989.

Tramblay, Y. and Somot, S.: Future evolution of extreme precipitation in the Mediterranean, Climatic Change, 151, 289 – 302, https://doi.org/10.1007/s10584-018-2300-5, 2018.

Tuel, A. and Eltahir, E. A. B.: Why Is the Mediterranean a Climate Change Hot Spot?, Journal of Climate, 33, 5829 – 5843, https://doi.org/10.1175/JCLI-D-19-0910.1, 2020.

Vanella, D., Longo-Minnolo, G., Belfiore, O. R., Ramírez-Cuesta, J. M., Pappalardo, S., Consoli, S., D'Urso, G., Chirico, G. B., Coppola, A., Comegna, A., et al.: Comparing the use of ERA5 reanalysis dataset and ground-based agrometeorological data under different climates and topography in Italy, Journal of Hydrology: Regional Studies, 42, 101 182, https://doi.org/10.1016/j.ejrh.2022.101182, 2022.

Varlas, G., Pytharoulis, I., Steeneveld, G.-J., Katsafados, P., and Papadopoulos, A.: Investigating the impact of sea surface temperature on the development of the Mediterranean tropical-like cyclone "Ianos" in 2020, Atmospheric Research, p. 106827, https://doi.org/10.1016/j.atmosres.2023.106827, 2023.

Verri, G., Furnari, L., Gunduz, M., Senatore, A., Santos da Costa, V., De Lorenzis, A., Fedele, G., Manco, I., Mentaschi, L., Clementi, E., Coppini, G., Mercogliano, P., Mendicino, G., and Pinardi, N.: Climate projections of the Adriatic Sea: role of river release, Frontiers in Climate, Volume 6 - 2024, https://doi.org/10.3389/fclim.2024.1368413, 2024.

Vicente-Serrano, S., Tramblay, Y., Reig Gracia, F., Gonzalez-Hidalgo, J., Beguería, S., Brunetti, M., Cindric Kalin, K., Patalen, L., Kržič, A., Lionello, P., Lima, M., Trigo, R., Kenawy, A., Eddenjal, A., Türkes, M., Koutroulis, A., Manara, V., Maugeri, M., Badi, W., and Potopová, V.: High temporal variability not trend dominates Mediterranean precipitation, Nature, pp. 1–9, https://doi.org/10.1038/s41586-024-08576-6, 2025.

Voldoire, A.: IPCC DDC: CNRM-CERFACS CNRM-CM6-1-HR model output prepared for CMIP6 CMIP, https://doi.org/10.26050/WDCC/AR6.C6CMCECC2, 2023a.

Voldoire, A.: IPCC DDC: CNRM-CERFACS CNRM-CM6-1 model output prepared for CMIP6 CMIP, https://doi.org/10.26050/WDCC/AR6.C6CMCECC1, 2023b.

Volodin, E., Mortikov, E., Gritsun, A., Lykossov, V., Galin, V., Diansky, N., Gusev, A., Kostrykin, S., Iakovlev, N., Shestakova, A., and Emelina, S.: IPCC DDC: INM INM-CM5-0 model output prepared for CMIP6 CMIP, https://doi.org/10.26050/WDCC/AR6.C6CMINIC0, 2023.

Wernli, H., Paulat, M., Hagen, M., and Frei, C.: SAL—A Novel Quality Measure for the Verification of Quantitative Precipitation Forecasts, Monthly Weather Review, 136, 4470 – 4487, https://doi.org/10.1175/2008MWR2415.1, 2008.

Wieners, K.-H., Giorgetta, M., Jungclaus, J., Reick, C., Esch, M., Bittner, M., Legutke, S., Schupfner, M., Wachsmann, F., Gayler, V., Haak, H., de Vrese, P., Raddatz, T., Mauritsen, T., von Storch, J.-S., Behrens, J., Brovkin, V., Claussen, M., Crueger, T., Fast, I., Fiedler, S., Hagemann, S., Hohenegger, C., Jahns, T., Kloster, S., Kinne, S., Lasslop, G., Kornblueh, L., Marotzke, J., Matei, D., Meraner, K., Mikolajewicz, U., Modali, K., Müller, W., Nabel, J., Notz, D., Peters-von Gehlen, K., Pincus, R., Pohlmann, H., Pongratz, J., Rast, S., Schmidt, H., Schnur, R., Schulzweida, U., Six, K., Stevens, B., Voigt, A., and Roeckner, E.: PCC DDC: MPI-M MPIESM1.2-LR model output prepared for CMIP6 CMIP, https://doi.org/10.26050/WDCC/AR6.C6CMMXML2, 2023.

Wilks, D.: Statistical Methods In The Atmospheric Sciences, vol. 59, Academic Press, https://doi.org/10.1016/S0074-6142(06)80036-7, 2006.

Xian, T., Xia, J., Wei, W., Zhang, Z., Wang, R., Wang, L.-P., and Ma, Y.-F.: Is Hadley Cell Expanding?, Atmosphere, 12, 1699, https://doi.org/10.3390/atmos12121699, 2021.

Xie, W., Yi, S., Leng, C., Xia, D., Li, M., Zhong, Z., and Ye, J.: The evaluation of IMERG and ERA5-Land daily precipitation over China with considering the influence of gauge data bias, Scientific Reports, 12, 8085, https://doi.org/10.1038/s41598-022-12307-0, 2022.

Xin, X., Zhang, J., Zhang, F., Wu, T., Shi, X., Li, J., Chu, M., Liu, Q., Yan, J., Ma, Q., and Wei, M.: IPCC DDC: BCC BCC-CSM2MR model output prepared for CMIP6 CMIP, https://doi.org/10.26050/WDCC/AR6.C6CMBCBCM, 2023.

Zappa, G., Hawcroft, M., Shaffrey, L., Black, E., and Brayshaw, D.: Extratropical cyclones and the projected decline of winter Mediterranean precipitation in the CMIP5 models, Climate Dynamics, 45, 1727–1738, https://doi.org/10.1007/s00382-014-2426-8, 2015.

Zeng, X. and Beljaars, A.: A prognostic scheme of sea surface skin temperature for modeling and data assimilation, Geophysical Research Letters, 32, https://doi.org/10.1029/2005GL023030, 2005.

Zhang, W., Villarini, G., Scoccimarro, E., and Napolitano, F.: Examining the precipitation associated with medicanes in the high-resolution ERA-5 reanalysis data, International Journal of Climatology, 41, E126–E132, https://doi.org/10.1002/joc.6669, 2021.

Ziehn, T., Chamberlain, M., Lenton, A., Law, R., Bodman, R., Dix, M., Wang, Y., Dobrohotoff, P., Srbinovsky, J., Stevens, L., Vohralik, P., Mackallah, C., Sullivan, A., O'Farrell, S., and Druken, K.: IPCC DDC: CSIRO ACCESS-ESM1.5 model output prepared for CMIP6 CMIP, https://doi.org/10.26050/WDCC/AR6.C6CMCSAE, 2023.

Zittis, G., Bruggeman, A., and Lelieveld, J.: Revisiting future extreme precipitation trends in the Mediterranean, Weather and Climate Extremes, 34, 100 380, https://doi.org/https://doi.org/10.1016/j.wace.2021.100380, 2021.